CHARACTERIZATION AND FABRICATION OF MWCNTs PRESSURE SENSORS FOR PRESSURE ULCERS MONITORING

by

Omer Faruk Firat

A thesis submitted to the Faculty of the University of Delaware in partial fulfillment of the requirements for the degree of Master of Science in Electrical and Computer Engineering

Summer 2017

CHARACTERIZATION AND FABRICATION OF

MWCNTs PRESSURE SENSORS FOR PRESSURE ULCERS MONITORING

by

Omer Faruk Firat

Approved: ____

Mark S. Mirotznik, Ph.D.
Professor in charge of thesis on behalf of the Advisory Committee

Approved: ____

Kenneth E. Barner, Ph.D.
Chair of the Department of Electrical and Computer Engineering

Approved: ____

Babatunde A. Ogunnaike, Ph.D.
Dean of the College of Engineering

Approved: ____

Ann L. Ardis, Ph.D.
Senior Vice Provost for Graduate and Professional Education

ACKNOWLEDGMENTS

First, I would like to express my gratitude to my adviser, Prof. Mark S. Mirotznik, for his support, guidance, and patience. Whenever I was in trouble about my research, and could not be able to see the next step, he was there with his advice to help me. I would also like to thank my colleges Nicholas Hudak, Benjamin Garrett, for their encouragement, kindness, and support.

I would like to especially thank Kaleb Burd, and Patrick Nicholson for helping to create the circuit design. Without their participation and input, the research could not have been successfully done.

I would like to give special thanks to Turkish Ministry of National Education for their financial support and encouragement throughout my Masters.

Lastly, I would like to dedicate this thesis to my family, my dear father Mahmut, beloved mother Bilge, and my sisters, Aysegul and Sevde Nur. They have been always with me with their fascinating support and love.

TABLE OF CONTENTS

LIST OF TABLES

LIST OF FIGURES

ABSTRACT

This thesis presents a low cost, flexible, scalable, and piezoresistive pressure monitoring system to prevent pressure ulcers. Pressure ulcer is one of the biggest health care problems in this century. Diabetes, obesity, becoming bedridden, and restricting a wheelchair are the main causes to pressure ulcer. A pressure monitoring system can help prevent this health condition. To implement a pressure sensor during experimentation, Multi Wallet Carbon Nanotube (MWCNT) and Polydimethylsiloxane (PDMS) were chosen as core materials. The array system was developed by using molding approach and additive manufacturing. Four different concentrations of MWCNTs were mixed by weight (2%, 2.5%, 3%, and 4%) in silicone elastomer; each were studied separately. The MWCNT-PDMS composite was fabricated as a parallel plate structure mode with 4x4 arrays.

The MWCNT-PDMS nanocomposite layer was sandwiched between two printed silver plates. Also, the electronic circuit was designed to get instant data from the array so that a color map can be created based on the pressure applied to the system simultaneously. The change in resistance value was observed when compressive forces were applied to the structures. A laser, nScrypt printer, and screen printer were utilized to fabricate this process. The piezoresistive pressure sensors were fabricated through a molding approach with a laser, and silver conductive plates were fabricated through an nScrypt printer. The first part of my thesis will explain a pressure ulcer, its causes-consequences, the devices that were used in this research overall and material properties and piezoresistivity feature. A number of samples were

fabricated to determine percolation threshold of the MWCNT-PDMS composite. The remainder of the thesis will outline the fabrication process and the circuit design. The results of the system will exhibit a color map of the applied pressure. This research can benefit those who have pressure ulcers risk, and millions of people can maintain their health and finances.

Chapter 1

INTRODUCTION

1.1 Motivation

Pressure ulcer is a sore that occurs due to blood flow interruption to a region of the body and the subsequent lack of oxygen in tissue, so soft tissue dies. Pressure ulcers are localized in skin and underlying tissue, which are usually heels, ankles, hips and tailbone. It may happen because tissues are squeezed between a bone, and cause limitations to change body positions for a long time. Pressure ulcers can occur in anyone, however, there are some groups whose risk to have pressure ulcers are higher. These people are bedridden and typically use wheelchairs, in which case their bodies stay in the same position for too long, seen in figure 1.1. Other groups who have higher risk of suffering these ulcers include the obese population whose vascular system has extra pressure, elderly people who have higher pain sensitivity thresholds, and diabetics, whose pain sensitivity is reduced and have restricted blood flow when facing high blood glucose levels that can increase fatty depositions on the walls of blood vessels [1].

Obesity and diabetes are associated with each other and obesity plays an important role in the cause of diabetes [2]. Obesity is measured by the body mass index (BMI), which is a classification method of adiposity estimation in adults, and a calculation of weight in kilograms divided by the square of the height in meters (kg/m^2) [3]. For example, a person whose weight and height are 80 kg and 1.80 m respectively will have 80 kg / (1.80 m) ^{2} = 24.69 BMI. Table 1.1 shows the international classification of adult obesity.

Table 1.1 The International Classification of Adult Obesity [2]

Classification	Body Mass Index	Risk of Co-morbidity
Normal	18.5-24.9	Average
Pre-Obese	25.0-29.9	Increased
Obese, Class I	30.0-34.9	Moderate
Obese, Class II	35.0-39.9	Severe
Obese, Class III	≥40.0	Very Severe

Obesity is a series global medical issue and one of the biggest public health problem in this century. Currently in the United States, approximately 38 % of Americans are considered obese [4]. While among men, the ratio is 30 %, among women, it is 40 % [4]. The overall ratio was 30 % in 2000, which demonstrates the increasing prevalence [5]. Worldwide obesity prevalence varies from 10 % in Belgium, 22 % in Turkey, to 27 % in England [6]. Obesity also has been increasing in children. This trend indicates no reduction in obesity prevalence, but an increase with a major impact on a variety of healthcare problems, containing in dermatology [31]. Several reports and papers published show the relationship between dermatology and obesity [31-34].

Obese people have extra adipose tissue, and existence of the adipose tissue increases the pressure and pain sensitivity threshold. Therefore, obese persons fell less pain when a force is applied such as pricking with a needle on their forearm [32].

Felling less pain and sensitivity decreasing causes pressure ulcers. It can be seen also in elderly people for the same reason, and in diabetics whose disease is a consequence of obesity.

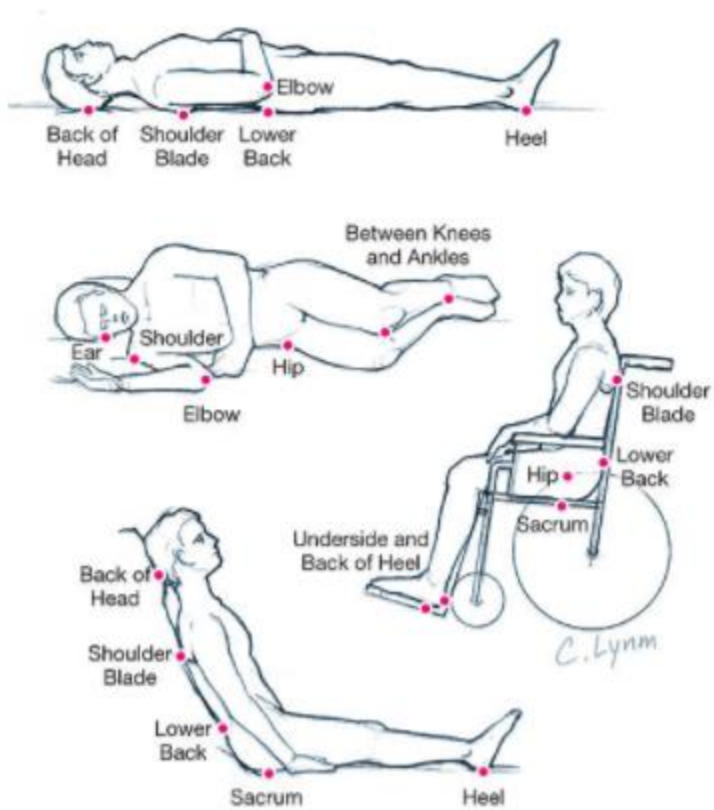

Figure 1.1: Common locations of pressure ulcers [39].

The presence of both obesity and diabetes increases the risk of having pressure ulcer and making it sustained particularly on the plantar side of feet [1]. AP Hills et al. studied plantar pressure differences between non-obese and obese adults and revealed that obese individuals have increased forefoot width and higher plantar pressures during standing and walking process [34]. Figure 1.2 shows obese and non-obese plantar pressure distributions while they are standing [34].

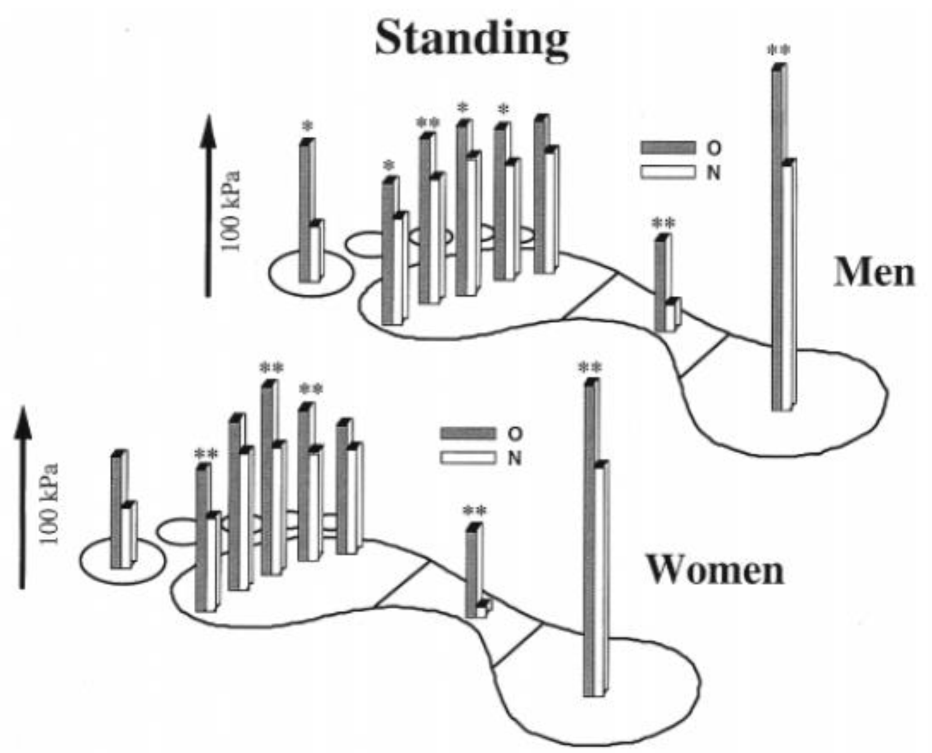

Figure 1.2: Plantar Pressure Distributions for obese and non-obese during standing. *P<0.05; **P<0.1 [34].

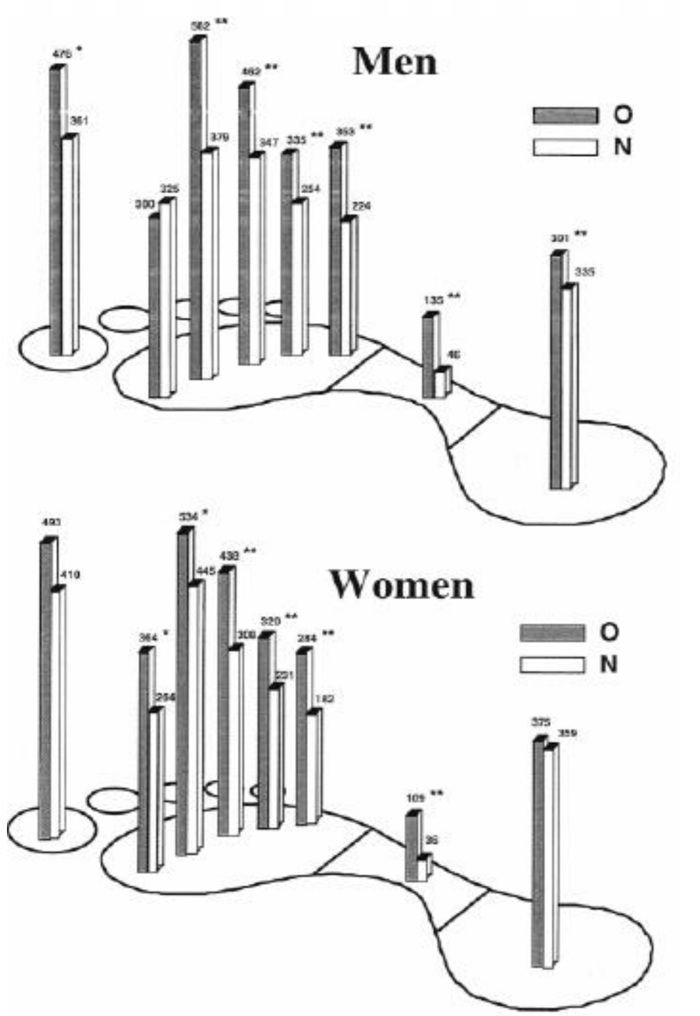

Figure 1.3: Plantar Pressure Distributions for obese and non-obese during walking [34].

As it can be seen from the figures, the peak pressure occurs under the longitudinal arch of the foot and metatarsal heads [34] where the pressure ulcers are seen on the plantar side of the feet.

The diabetic foot ulceration is a problematic and special condition of pressure ulcer which frequently ends up with amputation of the leg in the healing process.

Peripheral neuropathy and limited joint mobility cause unusual pressure loading on the foot [35], which leads to loss of sense of pain in the foot. Therefore, ulcers become chronic wounds and amputations are usually applied as a last treatment method.

National diabetes statistics report [36] indicates that 29.1 million people or 9.3 % of the American population have diabetes (diagnosed or undiagnosed). In 2010, around 73,000 non-traumatic lower limb amputations were performed in adults with diagnosed diabetes. Moreover, about 60 % of the all amputations among adults occurred in those who diagnosed diabetes [36]. The total estimated direct and indirect cost of diabetes in the United State was $ 245 billion in 2012 and $ 176 billion for direct medical cost and $ 69 billion for indirect medical cost e.g. disability, work loss, and premature death [36].

The total prevalence of venous stasis ulcers, diabetic foot ulcers, and pressure ulcers are between 3 to 6 million in the United Stated [37]. As it can be understood from the facts and statistics of pressure ulcers, it is one of the biggest healthcare problem in this century. To prevent pressure ulcers and suffering its pain and enormous cost to the society, a number of solutions such as pressure sensors have been studied. Some of which will be discussed below.

1.2 Applications

1.2.1 Printed Pressure Sensor Method for Plantar Pressure

C. Gerlach et al. introduced “Printed MWCNT-PDMS-Composite Pressure Sensor System for Plantar Pressure Monitoring in Ulcer Prevention” paper and fabricated printed pressure sensors to monitor plantar pressure. MWCNT-PDMS composite and conductive inks were fabricated through screen printing method. A gait analysis was accomplished to satisfy technical specification of the sensors. Measurement analyzing showed in the paper that it was possible to distinguish between unhealthy and healthy rollover patterns.

Six specific points on a human foot as seen in figure 1.4 [1] was detected and a fully printed insole, which contains six MWCNT-PDMS pressure sensors, was fabricated in order to obtain unhealthy rollover pattern.

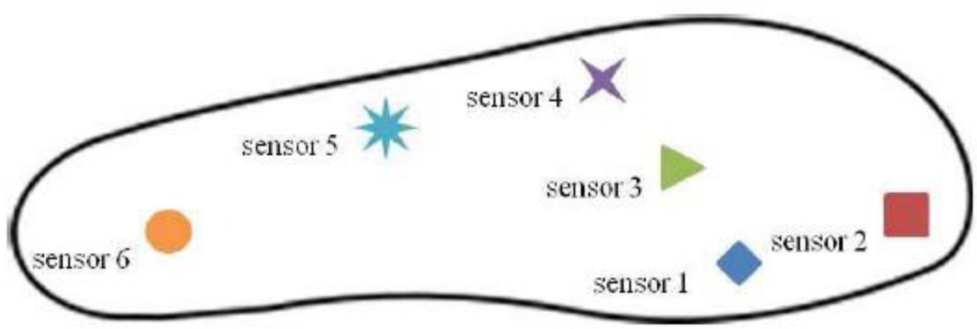

Figure 1.4: Location of the six sensors for the insole. Sensor 1 – medial forefoot, sensor 2 – hallux, sensor 3 – middle forefoot, sensor 4 – lateral forefoot, sensor 5 – midfoot, and sensor 6 – heel [1].

1.2.2 Piezoresistive Pressure Sensor Using Chemical Vapor Deposition Method

A Besoul, et al. investigated a carbon nanotube (CNT)-forest-based pressure sensor which was developed with the fabrication process of a Si-micromachining approach. They used Si substrate and made a Si nitride mask on both side of the substrate, then patterned a square window in the mask on the back side of the Si substrate. For the front side of the substrate, a molybdenum film was deposited with an electron beam evaporation method, and metal pads were patterned. To define where CNT forest grows which carried out with chemical vapor deposition, a catalyst layer was deposited. After CNT forest growing process, Parylene-C film was deposited to envelop the forest. Finally, dry etching process was applied [42]. The device design and fabrication sample are pictured in Fig 1.5 [42].

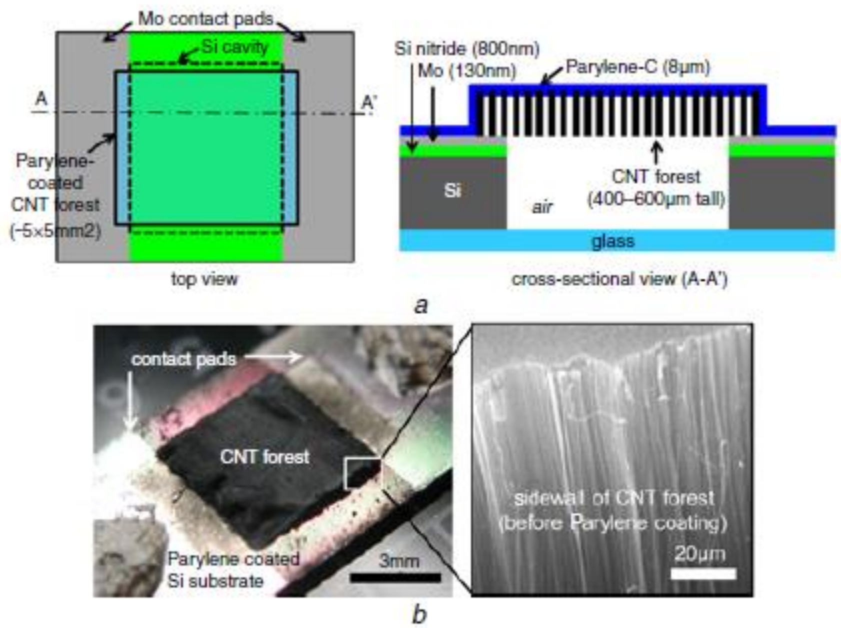

Figure 1.5: a) device design, b) fabricated sample device (left) with close-up CNT forest (rigt) [42]

As it can be seen from the above and other applications that they are expensive and complicated to implement on the human body specifically on plantar side. However, my research offers an alternative low-cost, flexible and scalable piezoresistive pressure sensor array to prevent pressure ulcers.

1.3 Contributions to Science

This thesis relays on current research about nanomaterial composites (Carbon Nanotube-epoxy), flexible-scalable pressure sensors with piezoresistivity features, and pressure ulcers. The pressure sensor system could be applied for preventing pressure ulcers on a human body specifically on a foot. Pressure sensor arrays can be fabricated through molding approach, which is low cost and easy to produce, and additive manufacturing, which contains a nScrypt and screen printer for narrow and large area applications respectively. Both technologies become a part of flexible and low cost electronics.

In this thesis, carbon nanotube based pressure sensor with its electronic circuit was investigated with a molding method and additive manufacturing. In this sense, 4x4 MWCT-PDMS piezoresistive sensor arrays and conductive pastes were fabricated via molding approach and nScrypt method respectively. Conductive inks (Silver) was printed with an nScrypt 3Dn-300 and two different sensor array patterns (different size and gaps) were fabricated through a molding technique by utilizing a laser. S. Khan et al. performed both conductive paste and composite fabrication via screen printing [26]. However, printing conductive paste via screen printer is not an efficient way in terms of consumption of this paste, because screen printer uses up a lot of conductive paste which increases the cost. On the other hand, nScrypt 3Dn-300 is more precise and consumes the just needed amount of ink. For these reasons, Silver ink was fabricated by the nScrypt 3Dn-300 printer. Also, a sample screen printed piezoresistive sensor fabrication was carried out for large area pressure distributions.

Additionally, both conductive ink and MWCNT/PDMS composite were printed by the nScrypt 3Dn-300 in order to compare the resolution of sensors with the molding approach. In the both approaches, PDMS and MWCNTs are sandwiched between Silver electrodes in a parallel state structure. The bottom electrodes, the composites and then the top electrodes are fabricated sequentially on a clear polyester film (PET) (McMaster- Carr). The top Silver ink is printed horizontally, and the bottom one is printed vertically.

Electronic circuit to scale a pressure distribution was carried out with a microcontroller, MOSFETs, and bit shifters. The resistance changing on individual sensor was showed as a voltage value. The 12-bit ADC of the CPU reads the voltage across the biasing resistor. The CPU transmits a 17-bit value back to the user's computer for processing by utilizing the UART connection. This 17-bit value contains the 12-bit ADC reading, a four-bit value for the location of the biasing sensor, and the last bit represents a stop bit. User's side is able to handle all the interpretation of the data. Additionally, the pressure distribution can be seen as a colorful image map using MATLAB. When pressure is first applied, or changed on the array system, the color scale, which consists of 4x4 colors on MATLAB, changes.

1.4 Additive Manufacturing

One of the fabrication techniques that were utilized in this research was additive manufacturing. Additive manufacturing has ability to fabricate direct and layer upon layer fabrication; It can be either adding materials on an existing structure or dispensing a material to a substrate in order to get a new structure. The additive manufacturing techniques employed in my research were nScrypt micro-dispensing and screen printing.

nScrypt printer can dispense a thermoplastic stock and also has a micro-dispensing feature. nScrypt 3D printer allows us to get complex geometries in contrast to conventional manufacturing methods. This feature enables the design of parts with intricate structure, and provides a variety of methods for small-batch fabrication of customized objects. Alternatively, screen printing is a technique that enables the fabrication of predetermined patterns onto substrate materials and this process can be repeated on subsequent substrates. Repeatability and getting fabrication in minutes are the most important properties of screen printing.

Additive manufacturing can facilitate the microstructural design and fabricate wide range of highly complex parts, enabling variety of engineering and biomedical applications [19]. Additive manufacturing has been becoming more common, advanced and reachable to more users from different areas. Multifunctional materials, printing techniques and smart design of complex systems are the three important keys to successful 3D printing.

In my research, an nScrypt 3Dn-300 (nScrypt Inc., Florida, U.S.) system was used to fabricate conductive inks and a molding method was used to create flexible pressure sensors. Alternatively, a screen printer (Nano Print Plus) was employed to sample large areas.

1.5 nScrypt Printer Overview

nScrypt 3D-300 is one of the printers from 3Dn series in nScrypt's 3D printer products and it is a multi-material additive printer (Figure. 1.6). This series overall has exceptional control, fine feature capacity and high speeds. These devices have a wide range of features such as micro-dispensing, 3D printing, laser micro machining, sintering, curing or heating, picking and placing, micro milling, UV curving, mapping and vision [27].

Figure 1.6: nScrypt 3D-300 system [27].

Users are capable of printing custom shapes with lighter weight, lower cost and better overall performance. It is possible to use multiple heads for different applications. Dual deposition heads enable simultaneous dispensation of two different materials. One head can dispense a thermoplastic stock and can print all the dielectric elements using the fused filament fabrication technique. (Figure 1.7) The only requirement here for nScrypt 3D-300 is that it has to be 1.75 mm filament. The second print head is for micro-dispensing process and is capable of printing any commercial or custom ink/paste (Figure 1.8). It can print lines as small as 20 microns [28]. In my research, micro dispensing technology is used to print conductive elements.

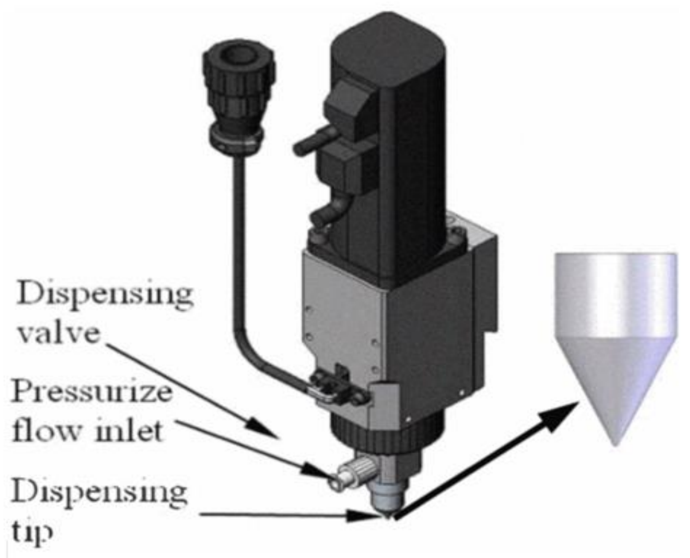

Figure 1.7: View of nScrypt smart pump

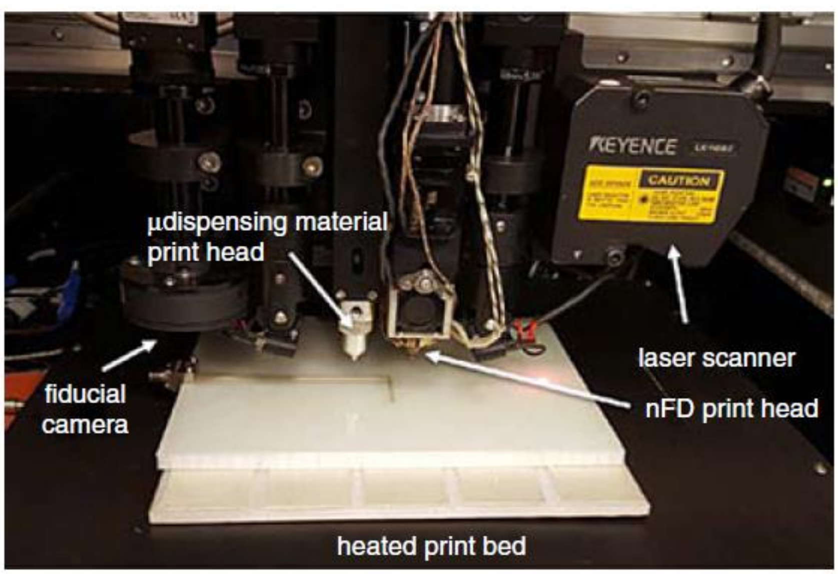

Figure 1.8: nScrypt 3D-300 multi-material printer [28].

1.6 Screen Printer

Screen printing is one of the fabrication technologies that utilizes a mesh screen, a flood and a squeegee (Figure 1.9). Users are capable of having their desired pattern on the mesh screen deposited onto a substrate. When the flood is activated, it spreads ink through the surface of the screen. Then, the system comes to right above the substrate, and then the squeegee starts moving and depositing the ink through the screen pattern onto the substrate [8]. After the fabrication process, the substrate is heated in order to make the printed ink cured. This fabrication process can be repeated with just placing a new substrate accurately. Therefore, users can produce mass fabrication of their desired pattern onto a substrate in minutes for a low cost.

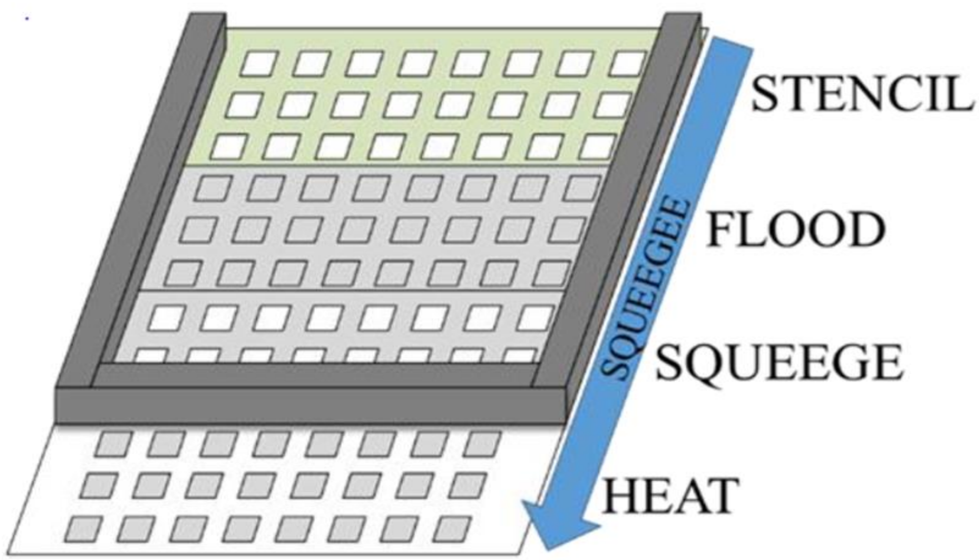

Figure 1.9: Flow of screen printing process [9]

Screen printing has been a mature technology in the industry for over 50 years. One of the big advantages of screen printing is having a stable process and low cost fabrication [29]. A number of materials have been developed in terms of electrical and physical optimum characterization for screen printer [30, 7]. Screen printing technology also has been used in a variety of applications such as flexible array sensors. The screen printer employed in my research was a Grafica Flextronica Nano-Print Plus with model number of GF-2228-N.P.P as seen in Fig. 1.10.

Figure 1.10: Grafica Flextronica Nano-Print Plus [8]

1.6.1 Screen Printing Manual

There are four modes to set up the system and its movements. These modes are actuated with a foot switch. This ability helps users calibrate and adjust the system before starting the fabrication process. It is necessary to step and release the pedal one time to activate each position of the control button. Up position of the button and step-release of the pedal makes the flood activate. Right position of the button brings the screen to the heated print bed so that users can adjust and place the substrate accurately. Down position of the button makes the squeegee actuate. Flood and squeegee bars that are connected to an actuating motor are standard. It is also possible to adjust the position and height of the flood and squeegee. Moreover, the flood and squeegee, whose set up is important to get a good and high resolution fabrication, have speed tuning for slow or fast printing.

1.6.2 Screen Printing Adjustments

In order to print a fabrication properly and efficiently, it is necessary to make some modifications on the screen printer. There are two basic adjustments for this issue. The first one is to set up the flood and squeegee properly. Having an adjusted flood and squeegee help apply equal pressure across the screen mesh so that the ink can be deposited through the mesh onto the substrate appropriately. The flood and squeegee can be modified with screws (Fig. 1.11). The second one for an appropriate fabrication is to set up a heat box (Fig. 1.11). It is essential to cure the printed ink on the surface [9]. The idea of setting up a heat box for the surface area is to protect the ink on the screen mesh from heat. Otherwise, before depositing the ink through the mesh, it would be cured, which is a not wanted case.

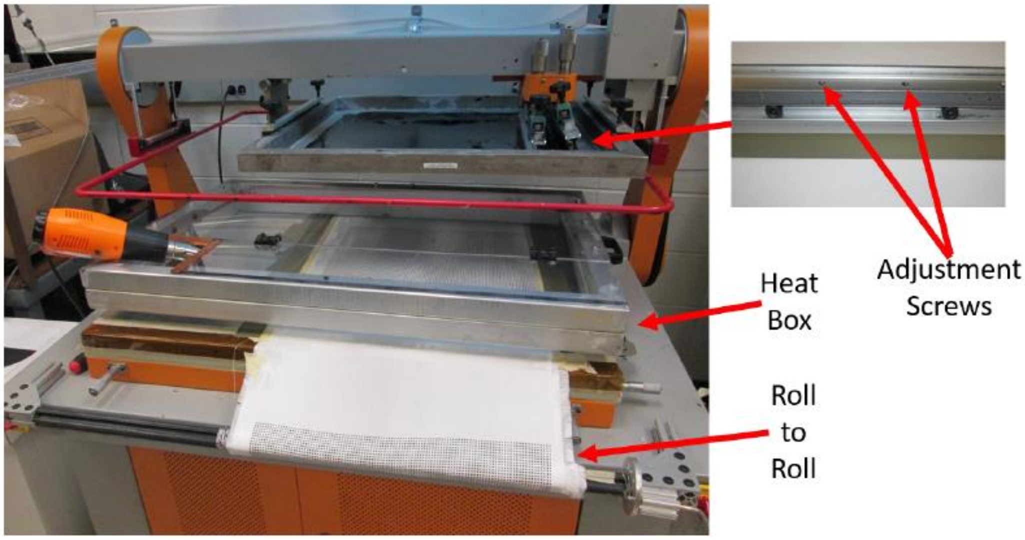

Figure 1.11**:** Screen printing adjustments [9].

1.7 Fabrication of Conductive Paste

The nScrypt microdispensing was used for the fabrication of small scale structures. DuPont CB028 Silver Conductive Ink was chosen as a conductive pate, and was printed through utilizing microdispensing smart pump. Four samples were fabricated by nScrypt microdispensing as seen pictured in Fig 1.12.

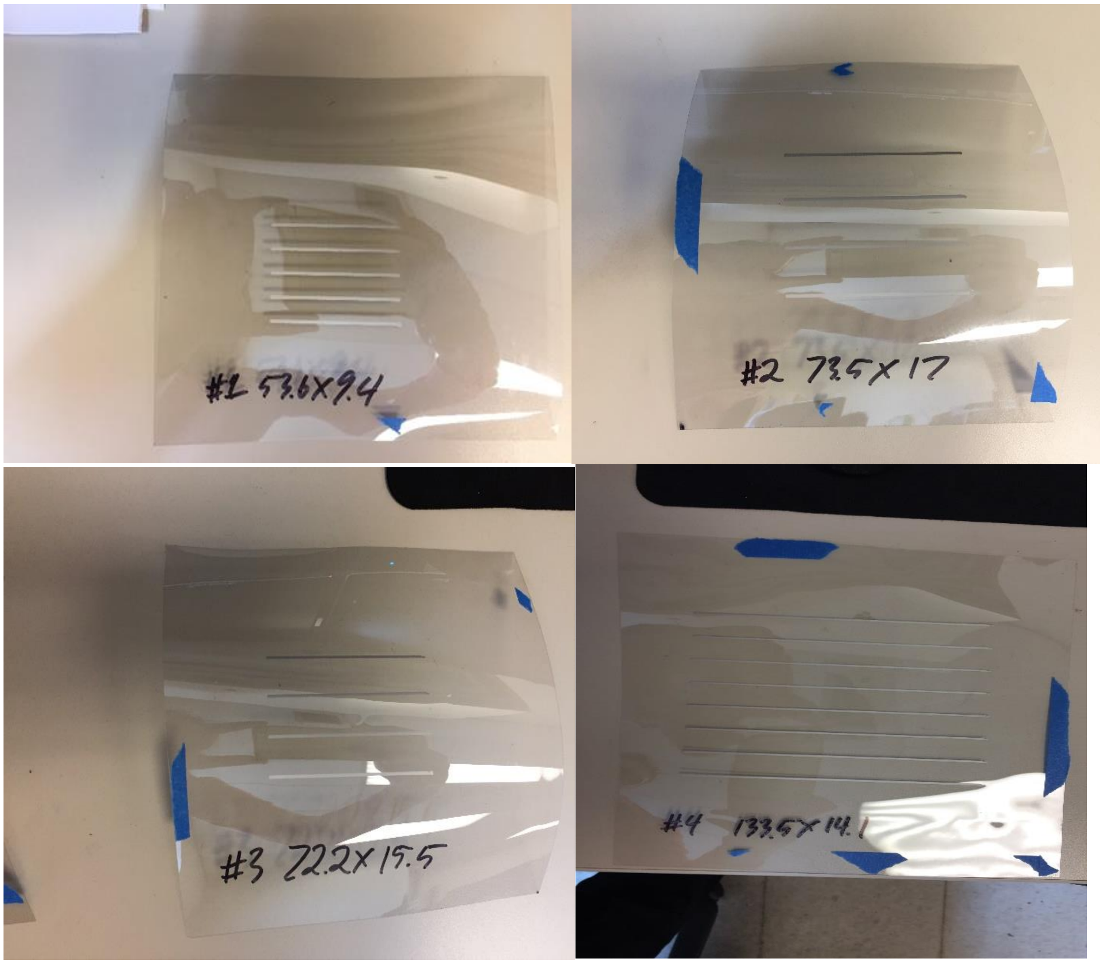

Figure 1.12**:** Sample fabricated Silver conductive inks

In order to get the desired structure from nScrypt, the samples were designed as a 3D model and the file was saved in Rhino software, which is pictured in Figure 1.13. Then, the file was converted to a readable g-code. This code was used to fabricate the pattern for the nScrypt. The substrate used was a clear polyester film as known PET, which is purchased from McMaster-Carr. Its tensile strength is 28 000 psi and thickness is 0.005 inch. As seen in the Figure 1.13, conductive inks were designed on the designed screen in order to figure out dimensions of the conductive inks easily and properly. The height and width of lines were 2 mm and 1 mm, respectively. The other measurements can be seen in the Table 1. Pattern (sensor) size refers to the length of one side of square pattern.

Table 2.1: Measurements of the Conductive Lines

Sample	**Pattern (Sensor) Size**	**Distance Between Conductive Lines**	**Conductive Line Length**	**Number of Line**
1	6.5 mm	15.5 mm	7.22 mm	4
2	3.5 mm	9.4 mm	53.6 mm	5
3	6 mm	17 mm	73.5 mm	4
4	5 mm	14.1 mm	133.5 mm	8

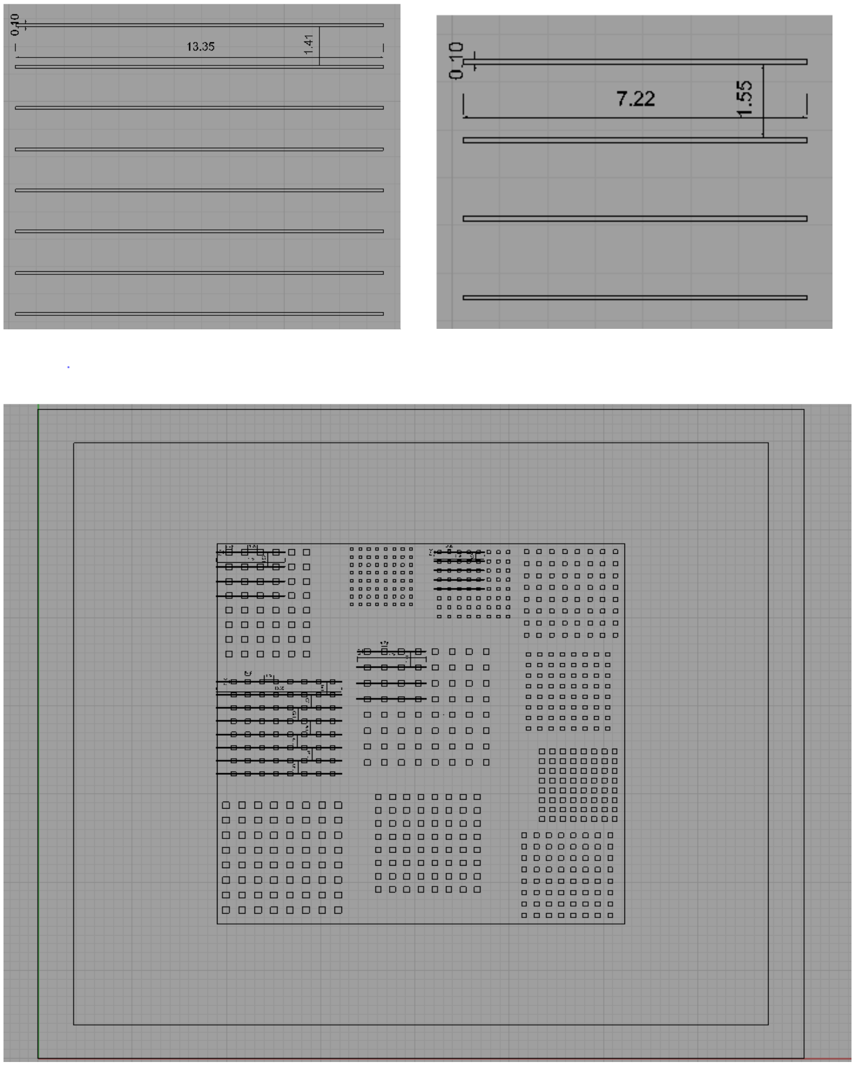

Figure 1.13**:** Conductive Ink Design

1.8 Fabrication of Pressure Sensors

1.8.1 Screen Printing Method

Desired pressure sensor patterns could be fabricated by using the screen printer after printing the conductive line samples onto a substrate. In my research, a sample screen printing fabrication was carried out and as a future work, a screen was designed which has different size of patterns. They are mentioned in detail in the future work part under chapter four.

As a sample fabrication, a screen was placed carefully and the modifications that were mentioned under the title of Screen Printing Adjustments were applied. The screen had a 28.5 degree stretch angle with a 325-mesh size which has 0.0011 inches width and a 0.001 inch emulsion thickness. The pattern was a square patch pattern and the size of the patch was 3 mm with a 4-mm period pictured in Fig. 1.15. The substrate was selected Dupont 2 mil Kapton film pictured in Fig. 1.14.

Figure 1.14: DuPont 2 mil Kapton film.

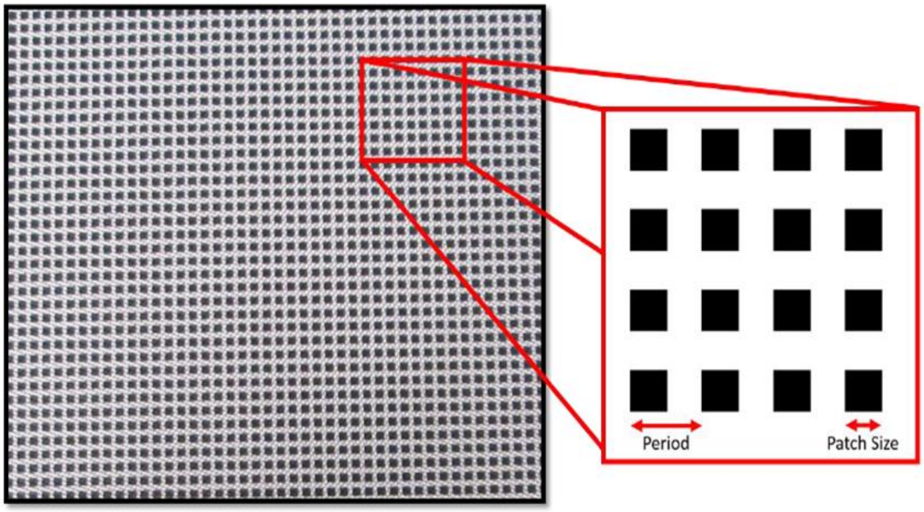

Figure 1.15: Screen printed pattern [8]

Piezoresistive sensors were fabricated on the substrate as seen in Fig. 1.16

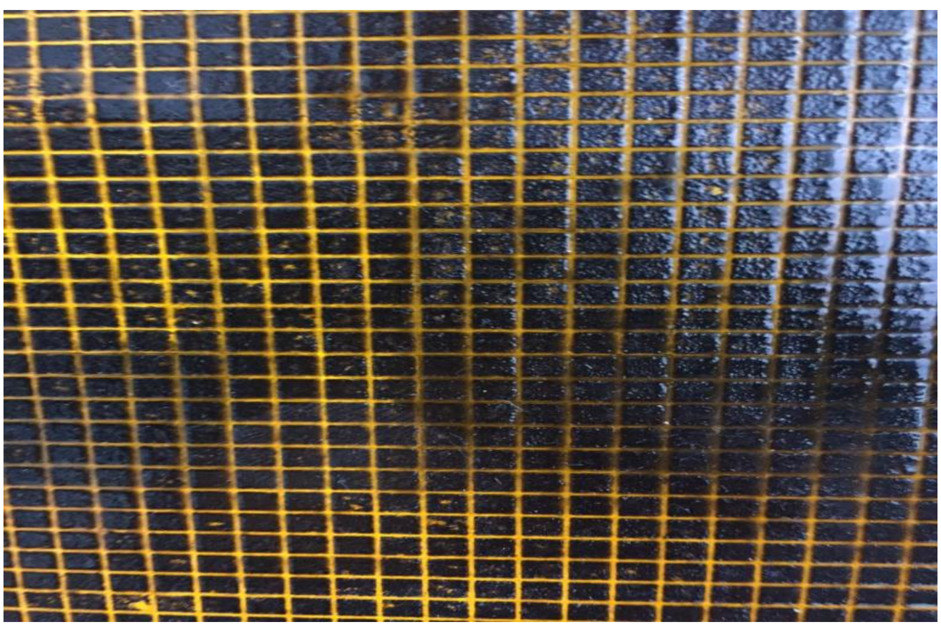

Figure 1.16: A sample screen printing fabrication.

1.8.2 Sensor Module Mold Fabrication Via Laser Cutting

The printed pressure sensors were fabricated via creating mold method. The desired designs of molds were first designed in Rhino software program, then a variety of materials with different thickness were cut in a laser. Paper, kapton film, and PET were the used materials. The designs of square molds were based on the dimensions of the conductive lines to match up with them. A full spectrum laser was employed for this fabrication process, pictured in Fig. 1.17. It is a H-Series CO_2 laser cutter, and has 20"x12" cutting area. It can cut materials up to 0.25 inch. Moreover, the machine can work with any program that prints such as AutoCAD, Rhino, Solidworks, PDF, and MS Word [43].

Figure 1.17: A full spectrum laser.

One of the cutting samples is pictured in Fig. 1.18. A PET substrate, which contains conduction lines for 5 mm square size sensor, was cut for 5 mm square size sensor molds.

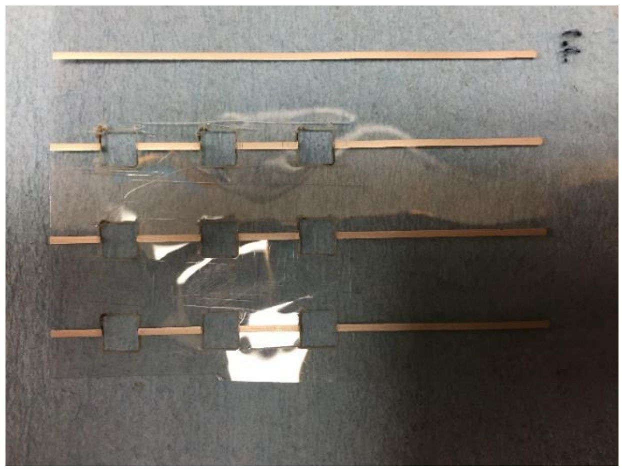

Figure 1.18: A sample mold

Chapter 2

MATERIAL CHARACTERIZATION AND STUDY FOR IDEAL PIEZORESISTIVE SENSING

2.1 Carbon Nanotubes

Carbon Nanotubes (CNTs) have been getting much attraction after they were observed over two decades because of their unique thermal, electrical and mechanical properties. CNTs have high aspect ratio (length over dimension) which is typically greater than 1000, low mass density, and high flexibility. CNTs can have higher conductivity than copper over long distances because CNT electrons don't get interruption significantly [10]. They have also extraordinary mechanical properties such that a high elastic modules and high strength which is 10-100 times stronger than steel [11]. CNTs which are seamless tubes with nonmetric diameters are graphene (a hexagonal lattice of carbon) sheets that are rolled up into a cylinder. Graphene is one carbon atom thick a planar sheet arranged in a two-dimensional honeycomb lattice (Figure 2.1).

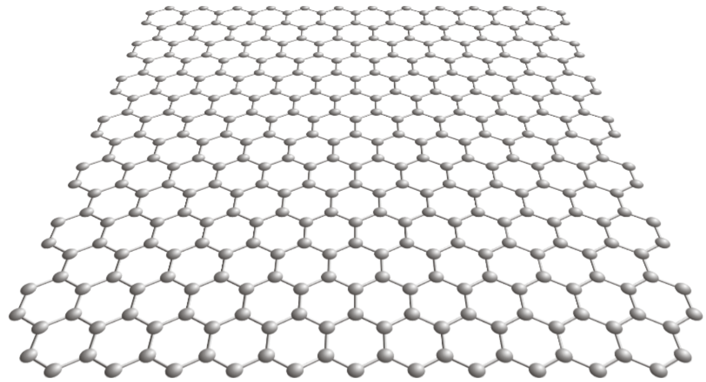

Figure 2.1: Graphene lattice

CNTs properties can be changed depending on the type of nanotubes and how they grow. The morphology of carbon nanotubes have quite variability and depend on synthesis and growth techniques and conditions. Different kind of nanotube morphologies exist. They can have a range from single walled carbon nanotubes (SWCNTs) and double walled carbon nanotubes (DWCNTs) to multi walled carbon nanotubes (MWCNTs) with a variety of diameters as seen in Fig 2.2. When a single sheet of graphite is rolled into a seamless cylinder, SWCNT can be synthesized. If the cylinders are inside a larger cylinder, then MWCNTs are created. Individual SWCNT could perform metallic or semiconductor behavior based on the nanotube growth process. When SWCNTs have different kind of atomic structure, this situation changes dimeter and electrical-mechanical properties of the nanotube structure [12].

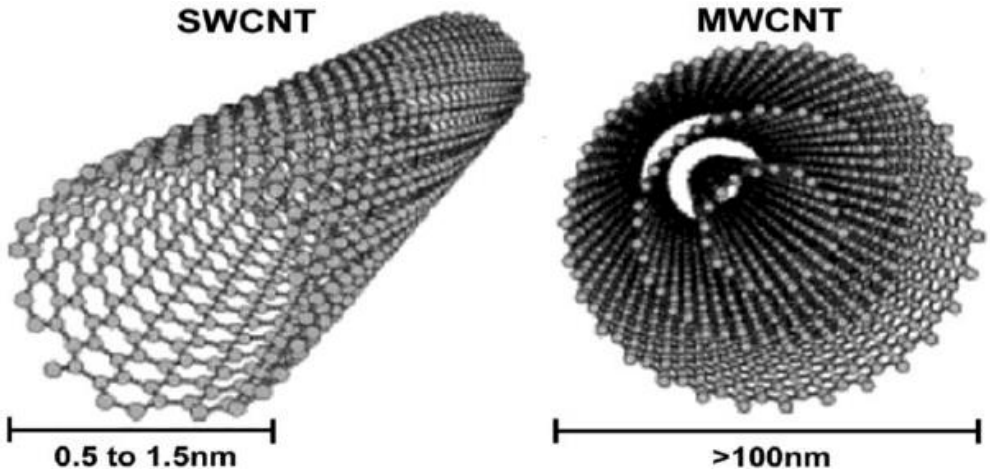

Figure 2.2: Structure of Carbon Nanotubes [13]

Since carbon nanotubes have extremely small dimensions and mass, they are usually filled into polymers. Z. Spitalsky et al. reviewed polymer nanocomposites filling with carbon nanotube research and listed a number of methods [10].

Polymers keep their characteristic properties such as flexibility, easy pressing and synthesis in conductive polymer composites which have similar trait to some metals and inorganic semiconductors [2]. Conductive polymer composites are operational for large area strains (±100% for elastomers), simple and their manufacturing is low cost although they have disadvantages of non-linearity, hysteresis and temperature drifts.

In my project, pressure sensing is carried out based on resistance changing of the composite. In order to have a sufficient resistance change in the composite, an appropriate CNT resistance network change is necessary under a mechanical force itself. A polymer matrix component embedded in CNT gives rise to achieve resistance chancing with CNT concentration. A low percolation threshold is aimed to preserve mechanical, electrical and physical properties of the polymer in CNT composite [15].

When low amount of loads such as a few newton is applied to the composite, a low elasticity modules of about 10 N/mm^2 of a poly material as a matrix component in the composite is necessary for enough amount of change of CNT network [14].

As advantages of CNTs, they have higher aspect ratio and lower percolation threshold which made them have a higher sensitivity than other filler materials such as carbon black or nickel nanoparticles [1]. The following graph shows the impact of CNT when it is mixed with carbon black. As it can be seen in the figure 2.3, with lower carbon contents we get higher tensile strength and lower surface resistance due to the CNT in carbon black. However, carbon black itself with high carbon contents cannot give as good results as CNT in carbon black material gives.

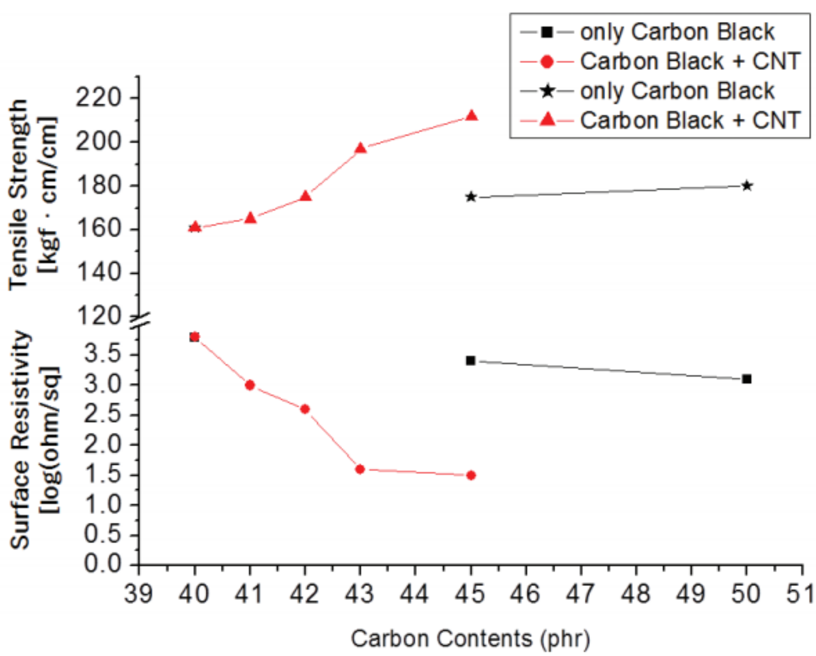

Figure 2.3: Carbon Black-CNT comparing [25].

PDMS is chosen as a polymer matrix element in MWCNT because MWCNT-PDMS has variety of exciting possessions that can be connected in sensor systems [16]. Beigbeder et al. [17] evaluated that PDMS builds strong CH-π bind with CNTs. PDMS is biocompatible for biomedical applications and has stable characteristic up to 300 C temperature [14]. PDMS consists of two components which are called part A and part B. Part A is linear base polymer with vinyl and part B is the cross-link agent. The ratio of parts is 10:1-part A and B, respectively. Part B is added in the end of a material process to make composite dry and hard.

In my research, a multi-walled carbon nanotube (MWCNT) - polydimethylsiloxane (PDMS) composite is presented. Recently, CNT embedded polymer composites have been studied and MWCT-PDMS composite is used in variety of material science research, Micro-Electro-Mechanical Systems (MEMS) devices, and printed, flexible electronics [1, 14, 18, 20, 26].

2.2 Piezoelectric, Capacitive and Piezoresistive Sensors

Pressure sensors are generally based one of the three basic principles which are piezoelectric, capacitive or piezoresistive. They recognize changes in electrical, resistance and capacitance respectively as a response to external pressure/force in flexible-printed sensors.

Piezoelectricity is an active phenomenon that use the generation of a voltage caused by an applied pressure and this method can be used for sensing of load/pressure. Piezoelectric sensors don’t require any external power supply. They operate dynamically and have wide application area in sensors, actuators and energy harvesters [21, 22]. They have high sensitivity measurement skill and are less sensitive to temperature impacts, however, their metrological analysis is complex and they are no capable of measuring statically.

S. Khan et al. [18] stated the importance of the Polyvinylidene fluoride (PVDF) and its copolymer Trifluoroethylene (TrFE) as piezoelectric materials and their widely usage due to their mechanical flexibility and ferroelectric characteristics. P(VDF-TrFE) has exiting properties such as high susceptibility, flexibility, cost effectivity, and allowing easy fabrication for sensing applications [23].

Capacitive pressure sensors are able to measure dynamically and statically and have high measurement reproducibility. However, capacitive pressure sensors are sensitive to humidity and noisy that brings complex filtering system to reduce the noise in the electronics.

Piezoresistive pressure sensors are capable of measuring both dynamically and statically with less sensitivity to noise. They have less complex electronic structure than piezoelectric and capacitive pressure sensors. In addition, piezoresistive sensors are simple, cost-effective, and printable and their spatial resolution is adjustable. However, they have disadvantages in terms of durability and drift compared to piezoelectricity and capacitive method [19].

The electromechanical properties of CNT allow it to be used as piezoresistors in mechanical sensors, such as gauges, strain, pressure sensors [18], [19], [24]. These piezoresistive materials frequently have low gauge factors and it brings a problem to develop piezoresistive devices. To solve this issue, conductive polymer composites have been figured out by incorporating piezoresistors with flexible platforms and CNT-PDMS is one of them.

2.3 MWCNT/PDMS Nanocomposite Preparation

The materials used to develop piezoreistive sensor arrays consist of multiwalled carbon nanotube (MWCNT) as a filler element, and polydimethylsiloxane (PDMS) as a matrix element. Here uniform dispersion of nanomaterials gives rise to have better sensor performance. As it was mentioned, MWCNT in PDMS matrix result gives rise to a number of exciting properties that can be connected effectively in sensors. Also, polymer nanocomposites have advantages of being simple, low cost, and effective for large strains.

Multiwalled CNTs (CM-95; Hanwha Nanotech, Korea) is entangled type, has 93~97% purity (wt. %) and has 0.05~0.1 bulk density (g/cc) as seen in the Figure 2.4 It is synthesized by catalytic CVD process. It has around 90 wt. % purity without any purification. In the synthetic process with some improvements, enhanced conductivity and dispersibility can be achieved for conductive composite applications.

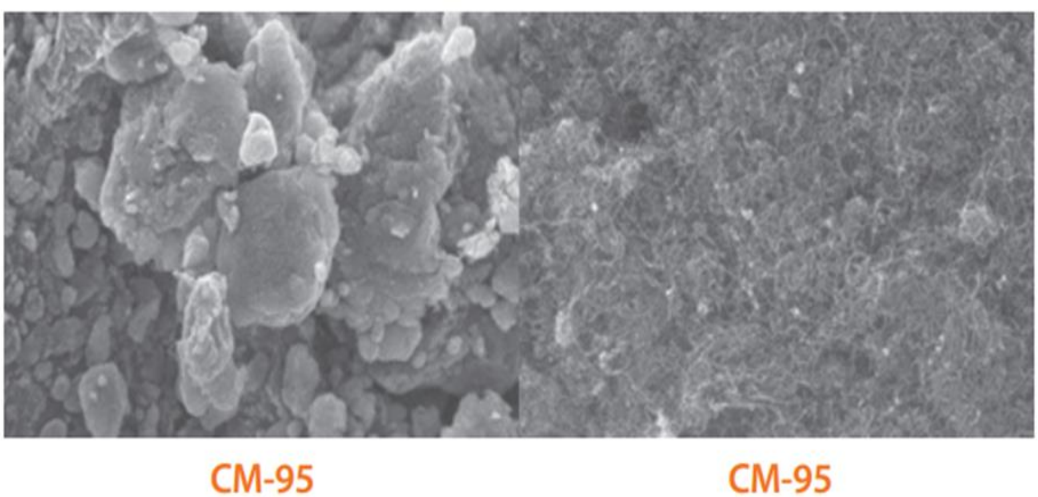

Figure 2.4: CM-95 Multi-walled Carbon Nanotube [25].

There are other MWCNT products available such as CM-130, CM-150, CM-230, and CM-250. While CM-95, CM-130, and CM-150 are for composite, CM-250 and CM-280 are for ink & paste. MWCNTs for composites have about 90 wt. % purity without any purification and have roughly $2x10^3$ aspect ratio. On the other hand, MWCNTs for ink & paste have nearly 95 wt. % purity without any purification and have roughly $2x10^4$ aspect ratio. CM-130 and CM-150 for composite materials are showed in Fig. 2.5 and Fig. 2.6 respectively. CM-95 was chosen in my research as a composite product based on CNT purity and price efficiency.

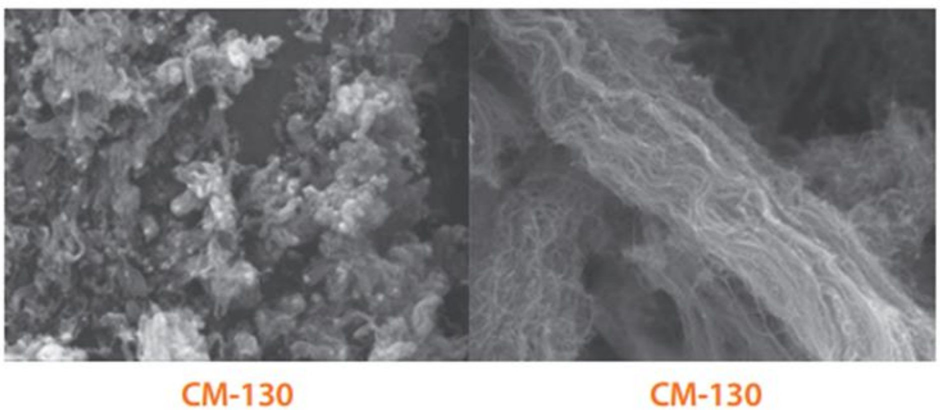

Figure 2.5: CM-130 Multi-walled CNT [25].

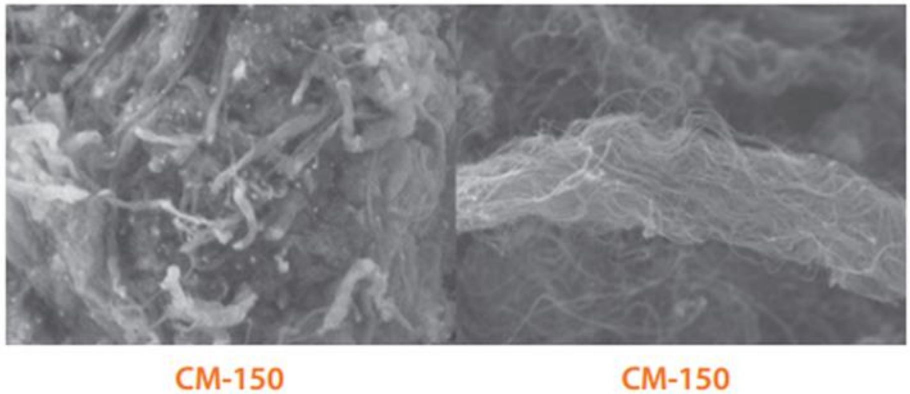

Figure 2.6: CM-150 Multi-walled CNT [25].

Additionally, CM-280 for ink materials is presented in Fig 2.7 below.

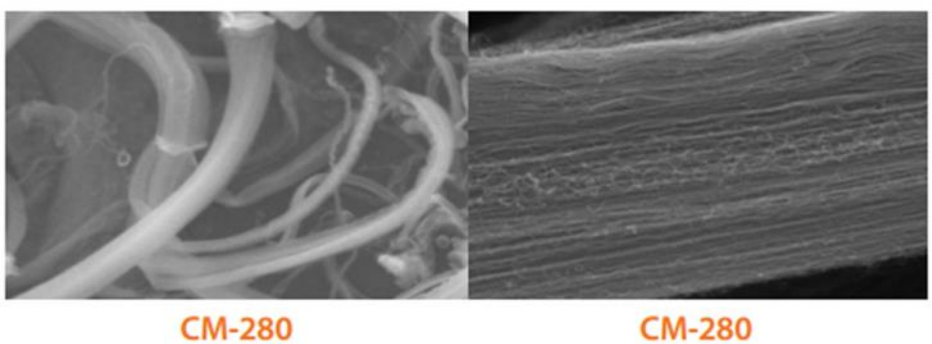

Figure 2.7: CM-280 Multi-walled CNT [25].

Table 2.1 shows specifications of MWCNT for composite products [25]. Moreover, Table 2.2 demonstrates specifications of MWCNT for ink& paste products [25].

Table 2.2: Specifications of Multi-walled CNT for ink & paste [25].

Property	**CM-95**	**CM-130**	**CM-150**
Type	Entangled	Aligned	Aligned
Purity (wt. %)	93~97	86~92	87~93
Bulk Density (g/cc)	0.050~0.100	0.025~0.050	0.030~0.070

Table 2.3: Specifications of Multi-walled CNT for composite [25].

Property	**CM-250**	**CM-280**
Type	Aligned	Aligned
Purity (wt. %)	92~96	96~99
Bulk Density (g/cc)	0.010~0.020	0.005~0.015

The MWCNT-PDMS composite was prepared based on the solution mixing method. In this dispersion, four different weight percentages of MWCNTs (2 wt.-%, 2.5 wt.-%, 3 wt.-%, 4 wt.-%) in PDMS matrix were obtained to get the low percolation threshold because it is an indication for usage of these kind of nanocomposites applications and it is beyond pressure sensor systems. Two percentage concentration of MWCNT was under the percolation threshold. However, other percentages (2.5, 3, 4) satisfied for development of pressure sensor. To guarantee the percolation network, 2.5 wt. % MWCNT was chosen for the composite.

2.5 wt. % MWCNTs were mixed with PDMS in a beaker by employing a magnetic stirrer as seen in Fig 2.8. This process was carried for 30 minutes.

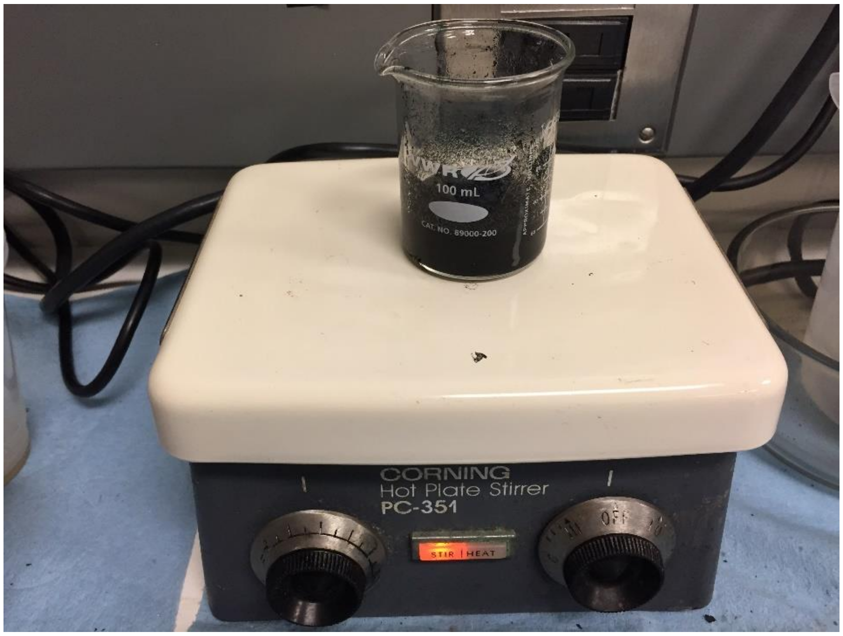

Figure 2.8: The composite mixture with a magnetic stirrer.

Then, an ultrasonic cleaner was used to have better composite resolution. When all fabrication processes were ready to fabricate the composite, part B of the PDMS was added to the composite. The magnetic stirrer was used again to mix the parts well for 15 minutes. After that, a degassing process was applied to the composite in order to move bubbles that were created during mixture process. The degassing vacuum and the pump are pictured in Figure 2.9.

Figure 2.9: Degassing process.

Now, it is ready to fabricate a sensor array via any fabrication method e.g. a molding or additive manufacturing approach.

Chapter 3

CIRCUIT DESIGN AND SENSOR ARRAY EXPERIMENTAL RESULTS

3.1 Pressure Distribution Measurement Circuit

To define applied pressure distribution on a system, an electronic circuit design was created. 4x4 pressure MWCNT-PDMS composite sensor array was connected to the circuit to obtain the signals of the 4x4 sensor array. The connection between circuit and the sensor array was carried out by eight wires whose four were merged to four columns, and the other four were merged to four rows.

The piezoresistive array iterator circuit has several operational sections, all of which are described below. The CPU first sends its clock signal and a data bit to the row bit shifter. The clock signal causes the bit shifter to shift through whatever data bit the row bit shifter receives. The data bit is a zero unless the fourth row is a one. In that case, the data bit becomes a high. The pattern that arises is one where a signal high starts in row one, shifts to row four, and repeats. Each of the outputs of the row bit shifter are attached to the gate of a MOSFET, while the drain is connected to five volts and the sources are each connected to an individual row of the piezo-resistive array.

The CPU sends a separate data bit to the column shifter, but the clock for this shifter comes from the output of the first row of the row shifter. In this case, the column shifter only shifts when the row shifter makes one complete cycle and returns to its start position. The data bit from the CPU produces the same effect for the column shifter, causing it to reset after all the columns have been traversed. Each output from the column bit shifter goes to the gate of a MOSFET, with the source connected to the biasing rheostat and the drain connected to an individual column of the piezo-resistive array. The rheostat is then connected to ground.

The array is set up in the following way, every element in the same row are shorted together and every element in the same column are shorted together. In the case of the piezo-resistive material, the tops of every element in the same row makes contact with the same trace, while the bottoms of every element in the same column makes contact with the same trace. In this set up, every element has its own individual row/column trace combination and the traces themselves, never intersect.

The N-Channel MOSFETs act as switches in this circuit. When they have 5V applied to their gates, they act as an open switch, and alternatively, as a closed switch when 0V are applied. Since the row and column bit shifters each only have a single high output each at any given moment, only a single row and column MOSFET is ever activated, and only one element in the array is every selected at once. This element is then effectively in a series circuit containing the source, the row MOSFET, the unknown piezo-resistance, the column MOSFET, the biasing resistor, and ground.

The 12-bit ADC of the CPU reads the voltage across the biasing resistor. Using the UART connection, the CPU transmits a 17-bit value back to the user’s computer for processing. This 17-bit value contains the 12-bit ADC reading, a two-bit value for the row number, a two bit value for the column value, and a stop bit. All interpretation of the data is handled on the user’s side.

3.2 Circuit Schematic and Its PCB Format

The electronic pressure measurement circuit schematic was designed in Autodesk Eagle software as in in figure 3.1. A PIC microcontroller, two MOSFETs, two bit shifters, a universal asynchronous receiver / transmitter connector, capacitors, and resistors were assigned in the electronic circuit.

Here, SSW-103-02-S-S, SSW-104-02-S-S, SSW-105-02-S-S, and SSW-106-02-S-S represent a connector tunable resistor with 3 sockets, 4 sockets for column and rows of the pressure sensors, a universal asynchronous receiver/transmitter with 5 sockets respectfully and they are all through-hole 0.025 inch SQ post sockets.

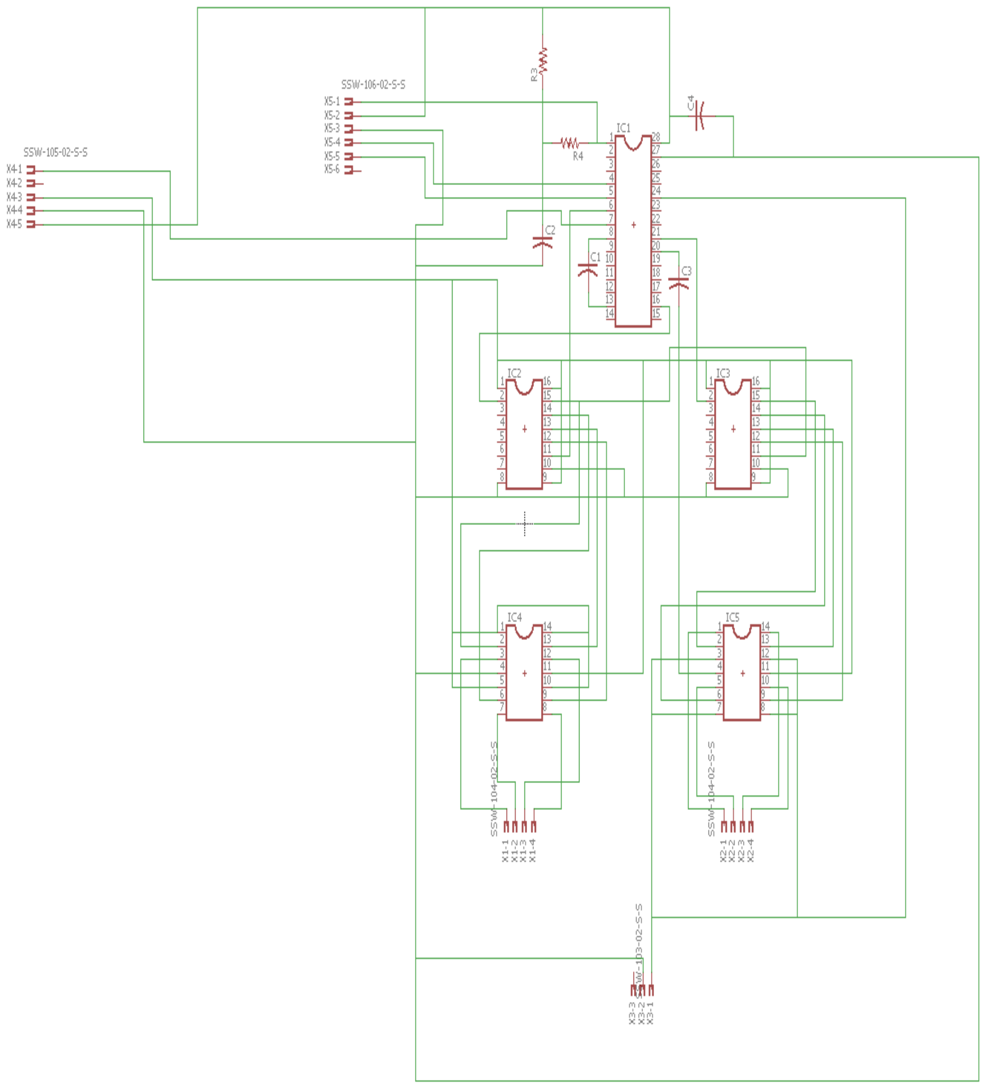

Figure 3.1: Schematic of the pressure measurement circuit diagram

After the schematic was designed, a PCB format of the schematic also was created. The PCB layout editor of Autodesk Eagle enable users to make annotations in the schematic and they are automatically updated in the PCB layout. Once the circuit works well and the layout is created, it is ready to fabricate it by PCB fabrication companies.

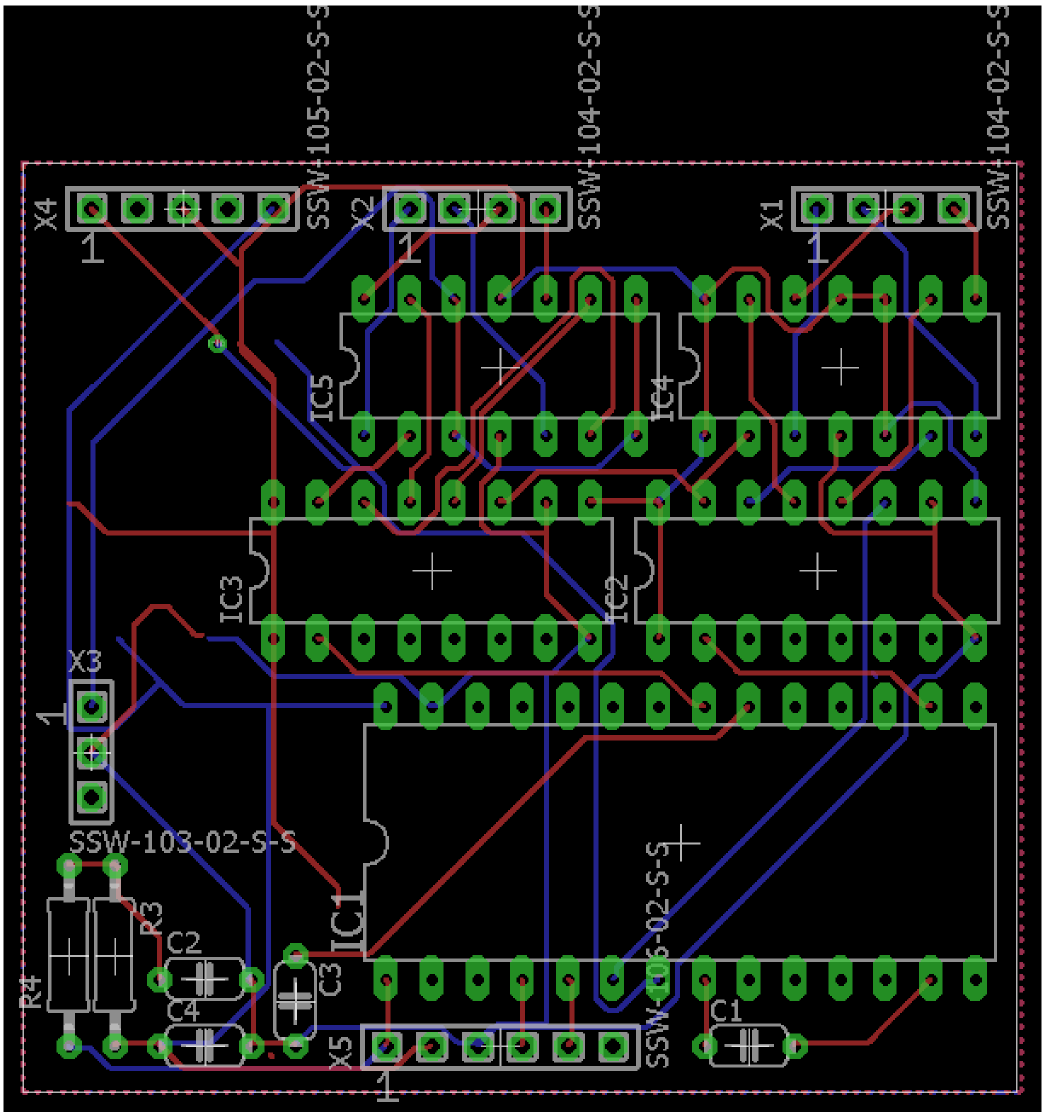

Figure 3.2: PCB design layout of the schematic diagram

3.3 Devices Utilized in the Circuit

3.3.1 PIC and Its Programming

The PIC microcontroller was selected from PIC24FJ microcontroller family as PIC24FJ128GB202 from Microchip Technology Inc. It has 20 input/output pins, and 128 KB program flash, and 8 KB data RAM memory. Also, it has 16 MIPS CPU speed and 16-bit architecture. Table 3.1 shows four members of PIC24FJ family with their specifications [38]. Fig. 3.3 shows pin diagram of PIC24FJ128GB202.

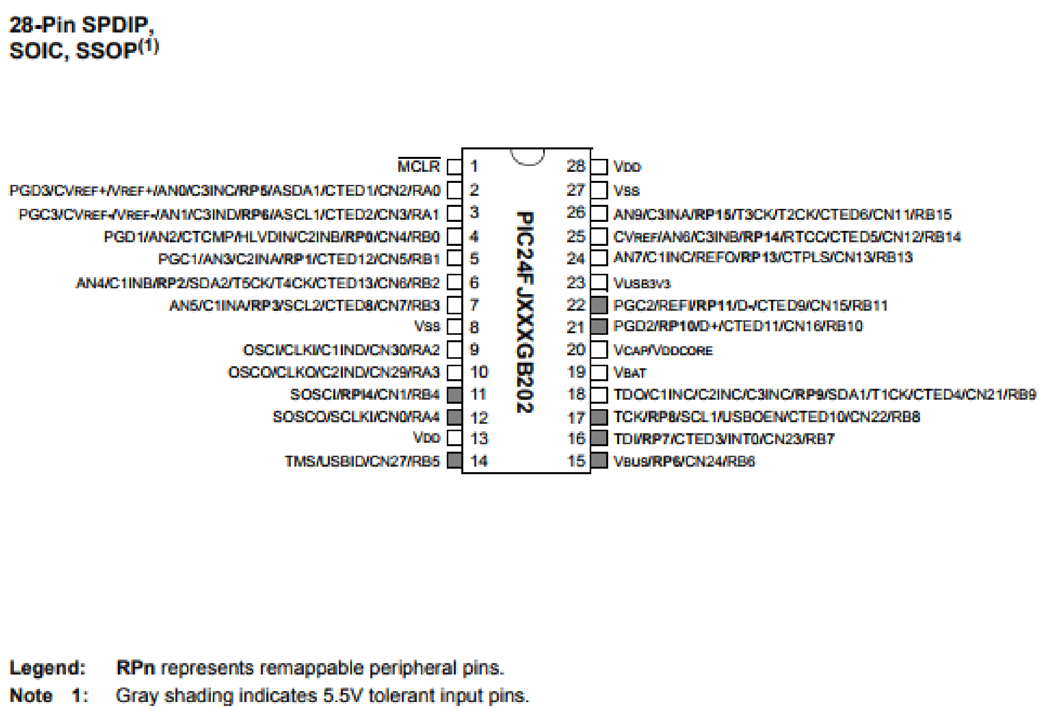

Figure 3.3 Pin diagram of PIC24FJ128GB202 [38].

Table 3.1: Features of PIC24FJ128GB204 Family [38].

Device	Memory		Pins	Analog Peripherals		Digital Peripherals							USB OTG	Deep Sleep w/VBAT	AES/DES Cryptographic
	Program Flash (bytes)	Data RAM (bytes)		10/12-Bit A/D (ch)	Comparators	CTMU (ch)	Input Capture	Output Compare/PWM	I^2C^{TM}	SPI	UART w/IrDA® 7816	EPMP/PSP	16-Bit Timers			
PIC24FJ128GB204	128K	8K	44	12	3	12	6	6	2	3	4	Y	5	Y	Y	Y
PIC24FJ128GB202	128K	8K	28	9	3	9	6	6	2	3	4	N	5	Y	Y	Y
PIC24FJ64GB204	64K	8K	44	12	3	12	6	6	2	3	4	Y	5	Y	Y	Y
PIC24FJ64GB202	64K	8K	28	9	3	9	6	6	2	3	4	N	5	Y	Y	Y

The PIC was programed via a PICkit 3 programmer / debugger from Microchip Technology, as seen in figure 3.3. It is a simple to use and low-cost device which is controlled by a PC running software program that is called MPLAB IDE. The MPLAB IDE is an interface that allows to access interactively all available features of the given device and make setup – modifications. The codes were used to program the PIC is also attached to my thesis in appendix.

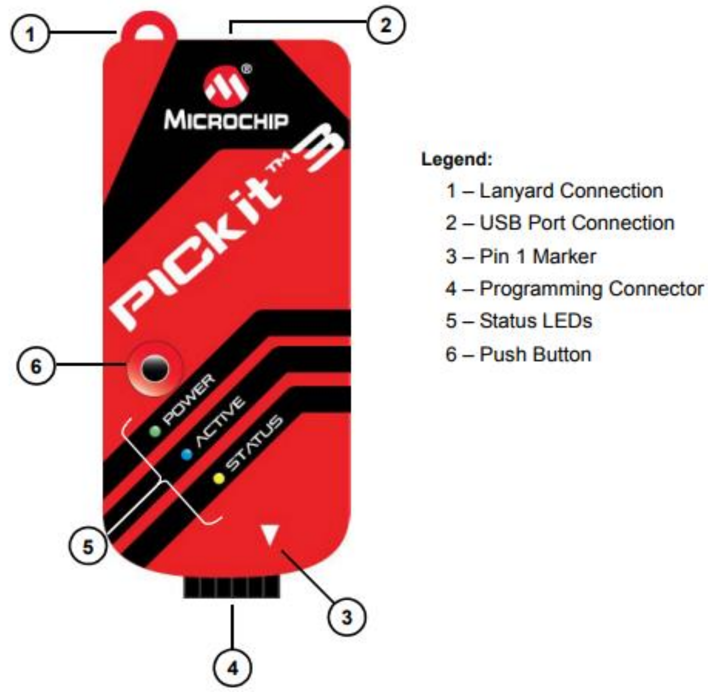

Figure 3.3: PICkit 3 programmer / debugger [40]

3.3.2 Additional Contributing Circuit Elements

The MOSFETs that are utilized in the electronic circuit were ALD1116, and monolithic dual N-channel MOSFET transistor arrays for analog applications. They have 0.7V threshold voltage, low input capacitance, and high input impedance around $10^{14}\,\Omega$ [41]. The pin configuration of ALD1116 dual N-channel MOSFET can be seen in figure 3.4.

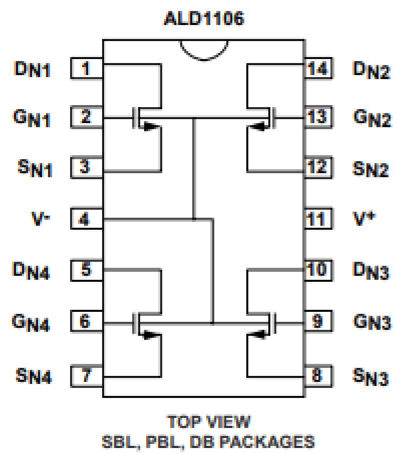

Figure 3.4: Pin configuration of dual N-channel MOSFET [41].

Two bit shifters, capacitors, resistors, and a tunable resistor were utilized in the circuit as well. The bit shifters basically shift a bit which comes from the PIC and transmits it to the gate of a MOSFET.

3.4 Voltage Reading

As it was explained, the 12-bit ADC of the CPU reads the voltage across the biasing resistor. This process was done with PuTTY software program. The serial port number, which is used for UART connection, and speed are set up before running the program, pictured in Fig. 3.5.

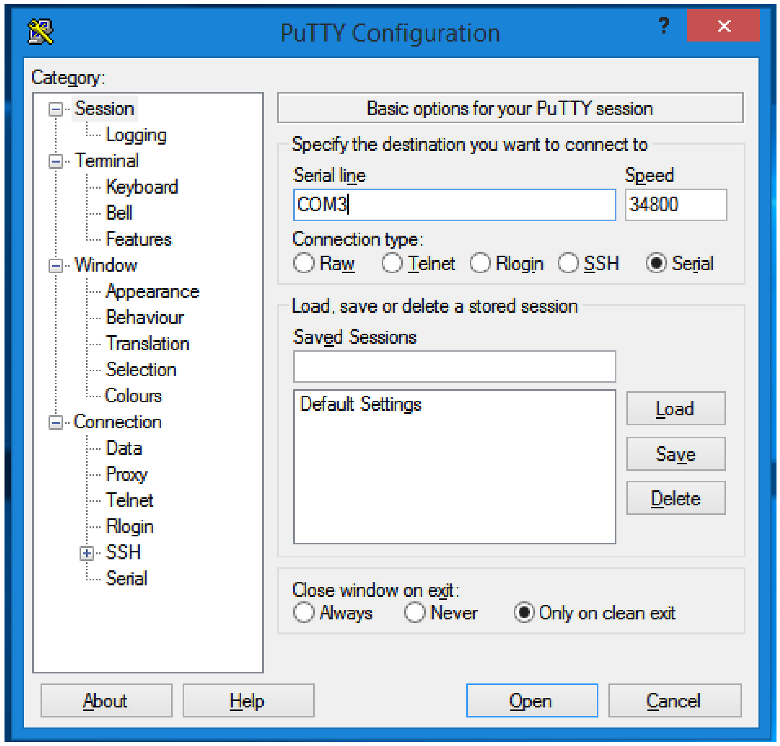

Figure 3.5: PuTTY Software Configuration.

Then, PuTTY gives a 17-bit value, which the CPU transmits back to the computer through UART link. This 17-bit value holds the 12-bit ADC reading, a two-bit value for the row number, a two-bit value for the column value, and a stop bit. A sample 17-bit value was pictured in Fig. 3.6.

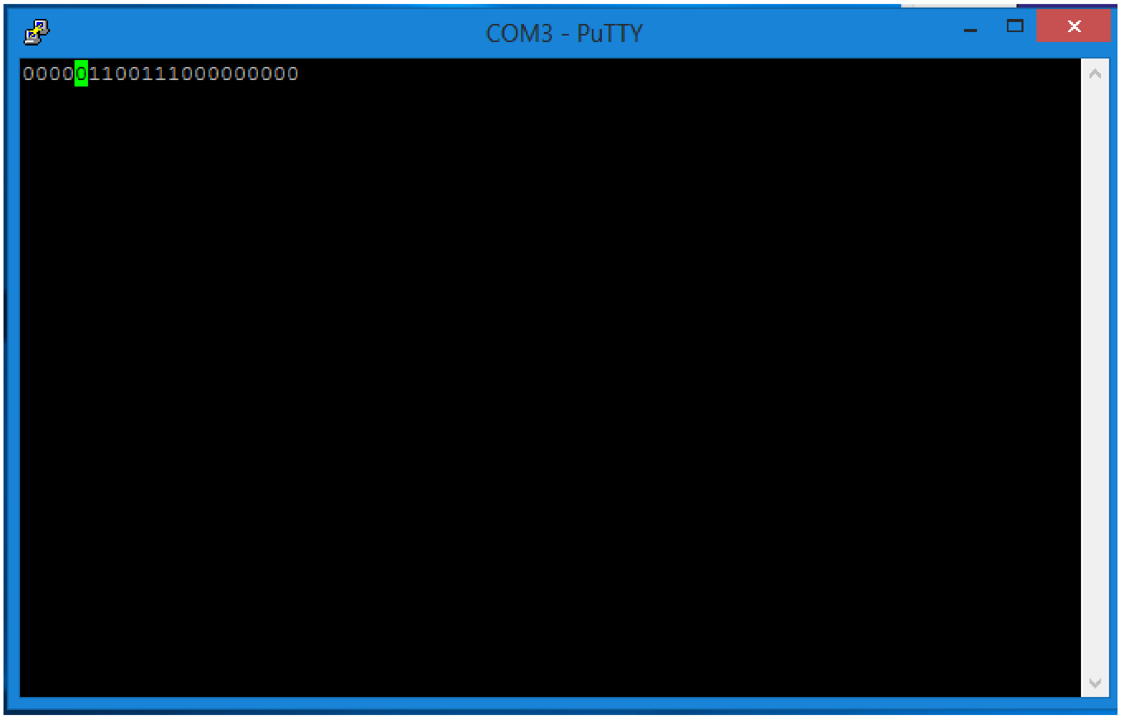

Figure 3.6: A sample 17-bit value

3.5 Displaying Image of the 4x4 Pressure Distribution

The voltage value of the biasing resistors displayed as a colormap with a color bar to understand scale of the voltage. It means scale of applied pressure at the same time. This prepossess was carried out with MATLAB.

There are 4x4 color cells in the colormap, which represent the 4x4 MWCNT-PDMS pressure sensor array. When there is no pressure to any sensor, it gives zero voltage outcome, which is symbolized by a blue color. When a pressure is applied to a sensor, the voltage value changes, so the color changes based on how much pressure was applied to the sensor. Some colormap pictures are showed in Fig. 3.7.

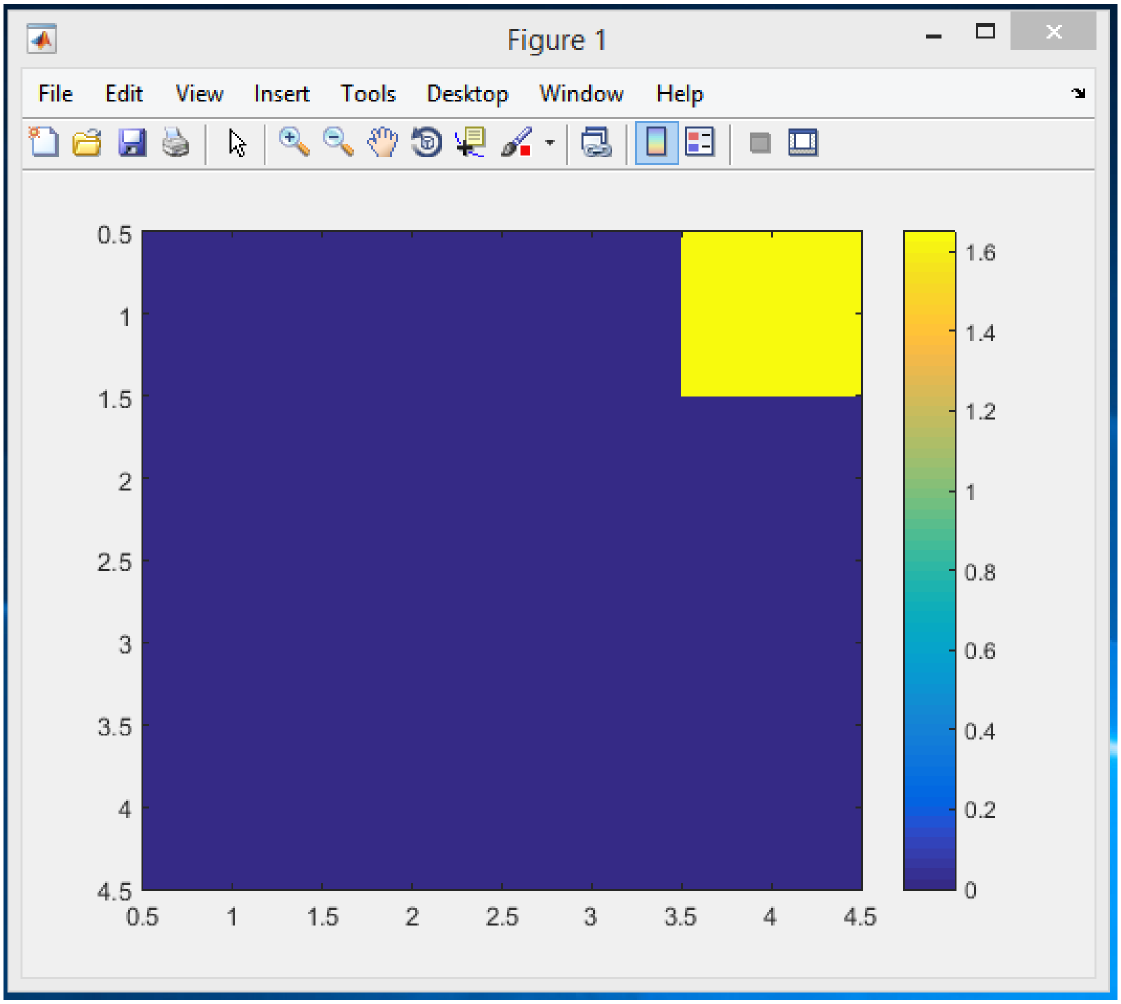

Figure 3.7: A sample color map

3.6 Experimental Response of MWCNT-PDMS Composite Sensors

The electrical response of the MWCNT-PDMS composites was observed by applying a compressive force on each module. When a force was applied to a composite sensor, a change in the electrical resistance was seen in the sensor, which satisfies the feature of piezo-resistivity.

Four different concentrations of MWCNT composites were investigated to define the most appropriate concentration of CNTs to maximize the change of resistivity seen by the sensor during compression. To implement this investigation, a custom made scale system was developed as pictured in Fig. 3.8.

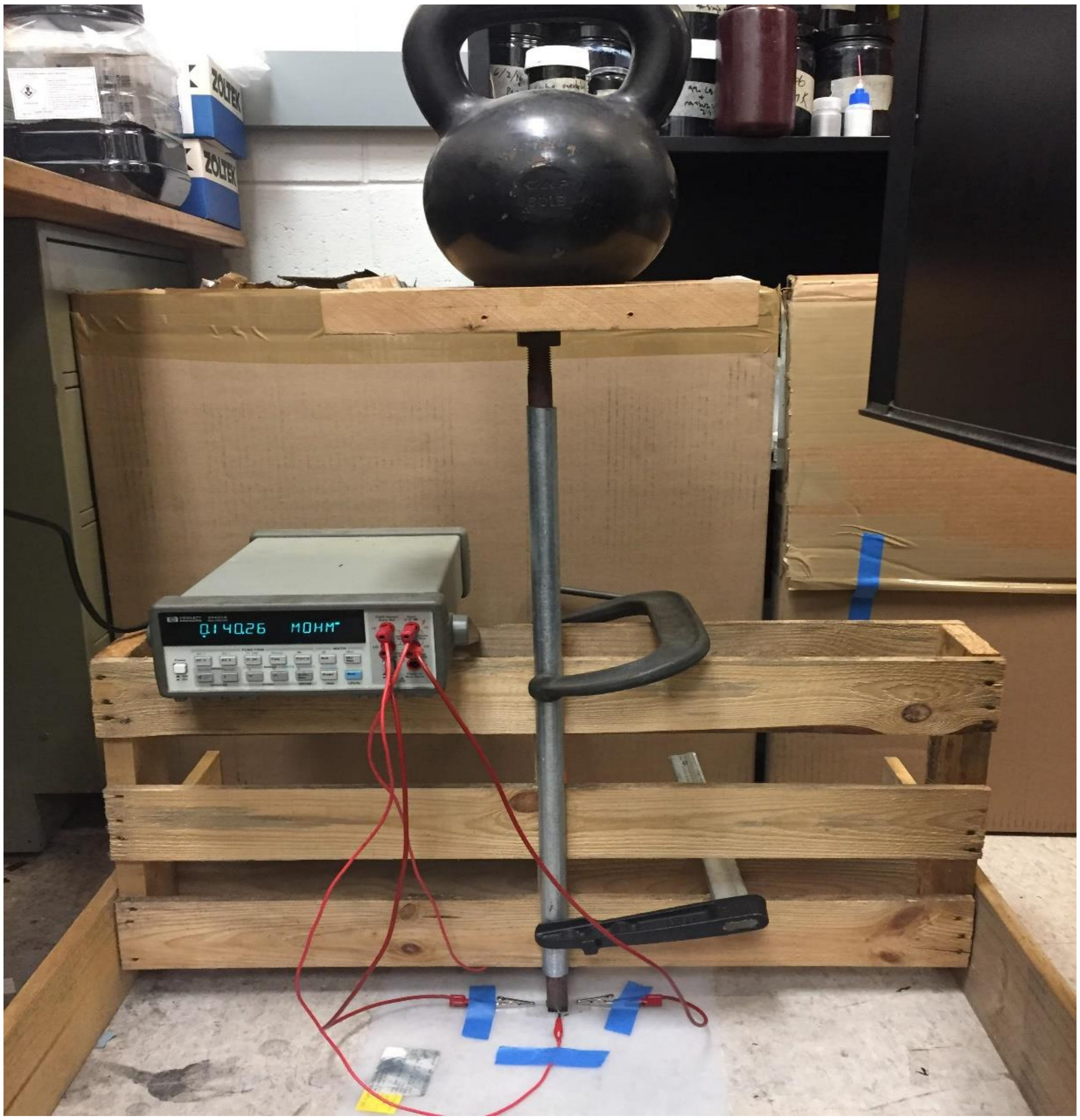

Figure 3.8: Custom made MWCNT sensor resistance monitoring system

The monitoring system consists of a 750mm long metal stick with an 18 mm diameter, 600 mm long metal pipe, 300 mm x 150 mm wood table, calibrated weights (5, 40, 65, 100 pounds), and a bench multi-meter. The wood table was fastened to the metal stick by using a drill and a nut, holding the metal pipe to the wooden frame. Then, the metal stick, which applies pressure onto a sample sensor, was placed into the metal pipe, causing a displacement of the wooden platform attached to the metal rod. Therefore, any calibrated weight can be applied to a MWCNT pressure sensor and its resistance change can be observed with the four-wire measurement method as seen in Fig 3.9. The sensor sizes that were used in this measurement experiment were 20 mm x 20 mm in order to match the diameter of the metal rod.

.

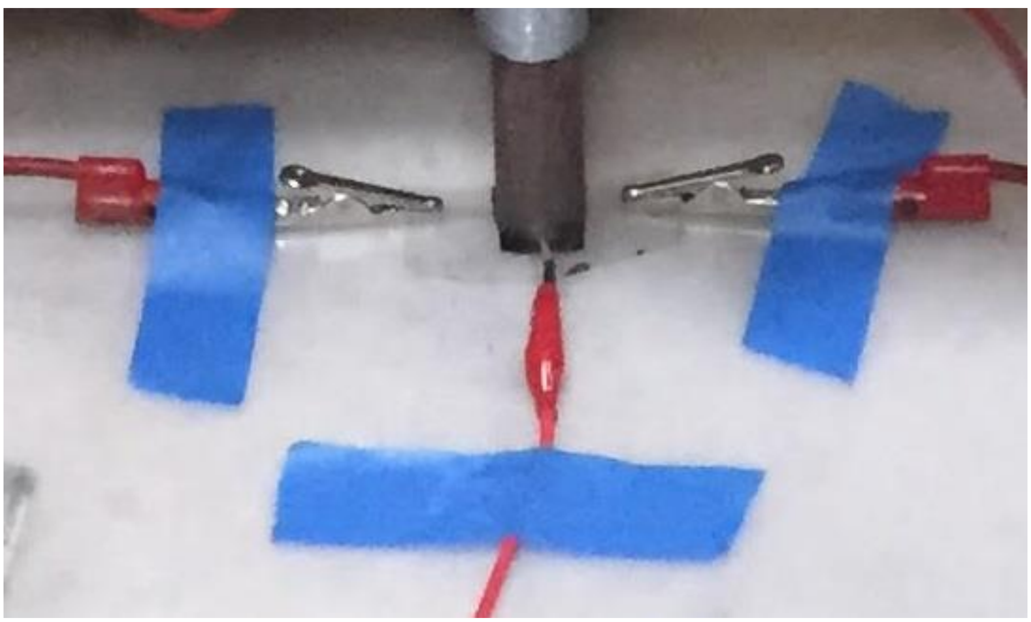

Figure 3.9: Four-wire resistance measurement method

First, the 2 % MWCNT concentration sensors were investigated, but no change in resistance was measured. The reason for this may be that the 2% concentration value was under the percolation threshold. Next, the 2.5 wt. % MWCNT concentration experiment was carried out with the calibrated weights, and different resistance values were obtained, pictured in Fig. 3.10.

.

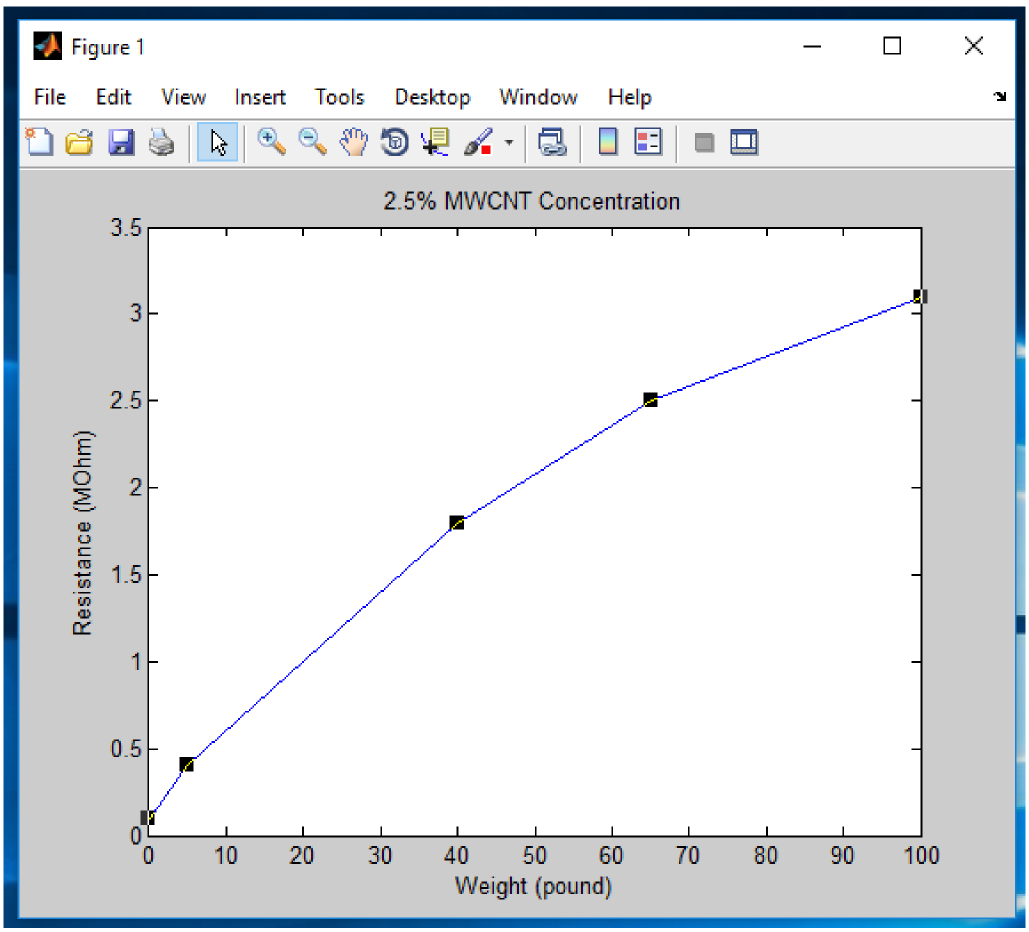

Figure 3.10: Resistance change vs. applied weight for 2.5 % MWCNT

The 3% concentration of MWCNT samples' sensor resistance behaviors with applied weights can be seen in Fig. 3.11.

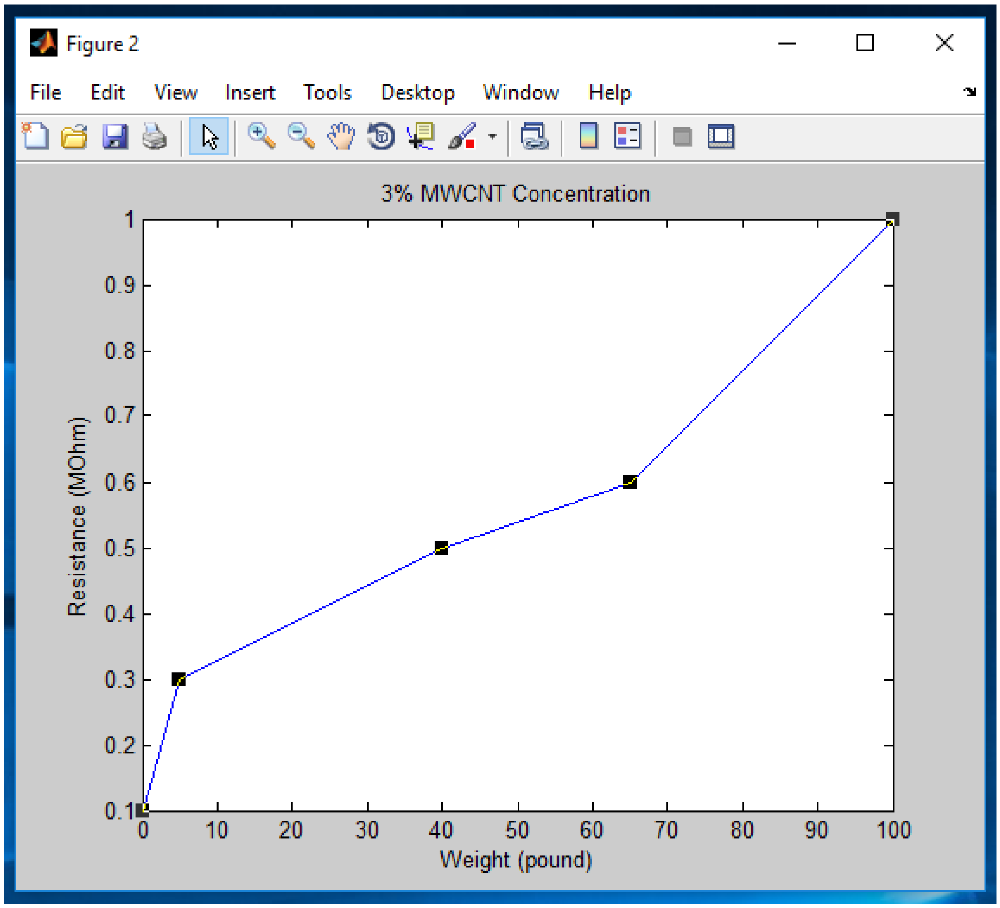

Figure 3.11: Resistance change vs. applied weight for 3 % MWCNT

Finally, the 4 % MWCNT concentration samples were tested to observe its resistance change, pictured in Fig. 3.12.

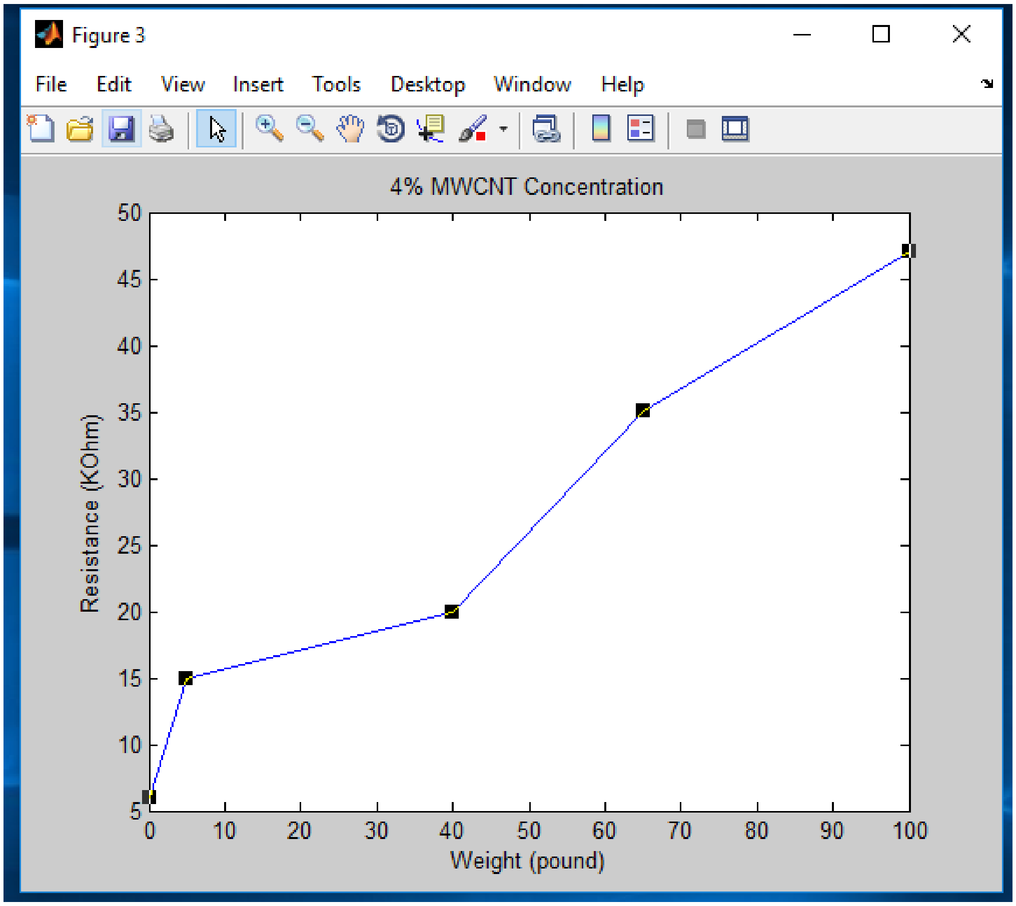

Figure 3.12 Resistance change vs. applied weight for 4 % MWCNT sensors

As it can be seen from the all three figures, the resistance increases with respect to applied weight, which confirms a piezo-resistive behavior. The most linear and accurate resistance was obtained from 2.5 % MWCNT sensors, so that concentration was chosen as the ideal concentration for optimally performing piezo-resistive sensing through MWCNTs.

Chapter 4

CONCLUSION

4.1 Summary of Work

This thesis demonstrates the causes and consequences of pressure ulcers, their possible precautions, applications, and results. Pressure ulcers are occurred because of diabetes, obesity, becoming bedridden, and restricting a wheelchair. Obesity and diabetes are related to each other and obesity is one of the strongest reasons for diabetes. The prevalence of obesity and diabetes has been increasing and as a result of this increasing, millions of people suffer from pressure ulcer. As a precaution of pressure ulcers, MWCNT pressure sensors for pressure distribution are presented in this research. Piezoresistivity, low cost, and being scalable are the major features of these pressure sensors.

Additive manufacturing and molding method were utilized to fabricate the conductive inks and pressure sensors respectively, and a 4x4 sensor array was fabricated. The circuit design, which was designed for the pressure distribution, gives a 17-bit value, which contains 12-bit voltage, 4-bit location, and a stop bit value. Resistance changing in a sensor was converted to a voltage value. Also, these values can be seen as a colormap with a color bar, which indicates the pressure distribution as a color map.

4.2 Future Work

Screen printer is convenient and low cost for large area printed pressure sensor array(s) fabrications. Since my research was aimed to focus pressure ulcer on foot, it was more efficient to use nScrypt printing and / or fabrication through laser by creating mold with desired dimension of the pressure sensors. As a large area applications, a hospital bed application could be considered, in which case it may be possible to get a pressure distribution of any patient while lying on the bed.

From this perspective, a screen was design and made fabricated on a frame. Grafica Flextronica Nano Print Plus allows to use different size of screen frames. In my research the screen had 29 inches by 32 inches frame size. Also, the screen had 3 mils emulsion thickness, 105.003 mesh size and 28.5 degrees stretch angle. The screen was designed by using Rhino CAD software program and purchased from UTZ manufacturing. Different size of arrays was designed on the same screen to define which array(s) will give a better fabrication. Arrays consist of 8 by 8 squares except one which is 6 by 8 because of the limited area.

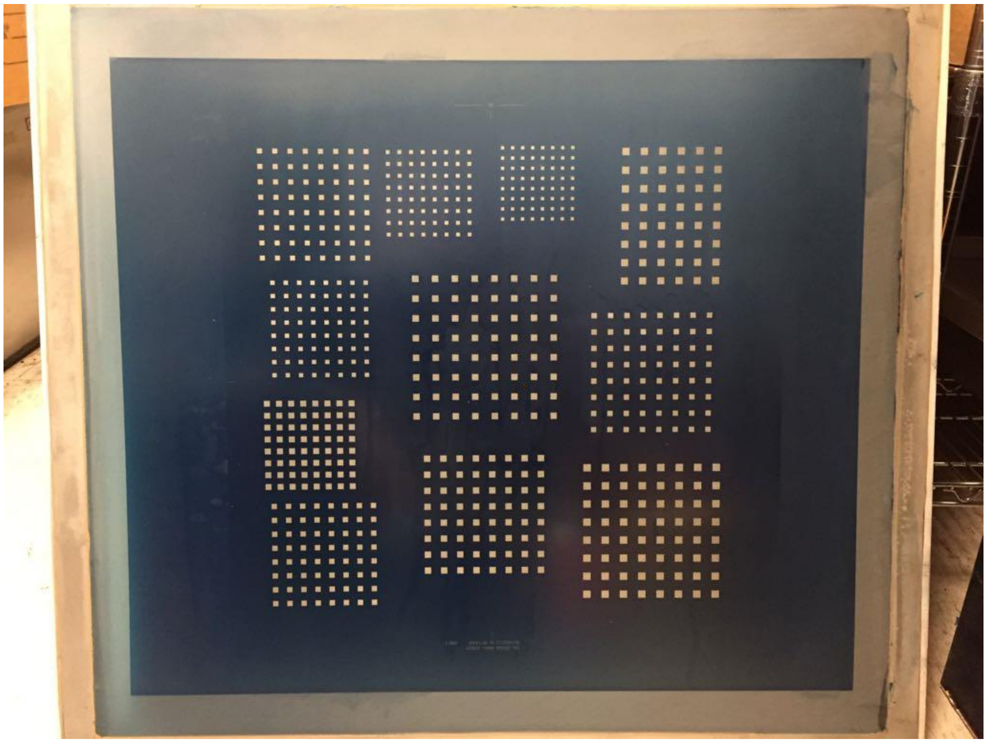

Figure 4.1. Screen Design

A square patch pattern was chosen to design the screen by consisting of 8 by 8 and 6 by 8 arrays. Each array has different size of patch while the period is the same in the array. For example, in one array squares have 5 mm length and 10 mm distance between two squares as seen in Fig. 1. 7. In the screen design 3, 3.5, 4, 5, 6, and 6.5 mm square size and 6, 7, 8, 10, 12, 12 mm distance between squares respectively are available. Why the square distance is chosen 2 times bigger than the length of square is because to prevent cross talking between the sensors.

REFERENCES

1. C. Gerlach *et al*., "Printed MWCNT-PDMS-Composite Pressure Sensor System for Plantar Pressure Monitoring in Ulcer Prevention," in *IEEE Sensors Journal*, vol. 15, no. 7, pp. 3647-3656, July 2015.

2. King Sun Leong, John P. Wilding, Obesity and diabetes, Best Practice & Research Clinical Endocrinology & Metabolism, Volume 13, Issue 2, 1999, Pages 221-237, ISSN 1521-690X.

3. "WHO :: Global Database on Body Mass Index", *Apps.who.int*, 2017. [Online]. Available: http://apps.who.int/bmi/index.jsp?introPage=intro_3.html. [Accessed: 31-Jul- 2017].

4. Flegal KM, Kruszon-Moran D, Carroll MD, Fryar CD, Ogden CL. Trends in Obesity Among Adults in the United States, 2005 to 2014. *JAMA.* 2016;315(21):2284-2291. doi:10.1001/jama.2016.6458

5. Flegal KM, Carroll MD, Ogden CL, Johnson CL. Prevalence and Trends in Obesity Among US Adults, 1999-2000. *JAMA.* 2002;288(14):1723-1727. doi:10.1001/jama.288.14.1723

6. World Obesity Federation | Data", *Worldobesity.org*, 2017. [Online]. Available: http://www.worldobesity.org/data/.

7. I. El Houti El Jazairi, T. Thierry, and J.-P. Moliton, “OTFT with silk screen printed drain and source,” *Micro Nanosyst.*, vol. 1, no. 1, pp. 46–49, 2009.

8. M. Mills, "Additive manufacturing of RF absorbers", M.S., University of Delaware, 2016.

9. Mark S Mirotznik, “Advanced Multifunctional Materials for High Speed Combatant Hulls,” *Defense Technical Information Centre*, 2015.

10. Zdenko Spitalsky, Dimitrios Tasis, Konstantinos Papagelis, Costas Galiotis, Carbon nanotube–polymer composites: Chemistry, processing, mechanical and electrical properties, Progress in Polymer Science, Volume 35, Issue 3, 2010, Pages 357-401, ISSN 0079-6700.

11. Erik T Thostenson, Zhifeng Ren, Tsu-Wei Chou, Advances in the science and technology of carbon nanotubes and their composites: a review, Composites Science and Technology, Volume 61, Issue 13, 2001, Pages 1899-1912, ISSN 0266-3538.

12. Carbon Pandey, G., & Thostenson, E. T. (July 01, 2012). Carbon Nanotube-Based Multifunctional Polymer Nanocomposites. *Polymer Reviews, 52,* 3, 355-416.

13. Malhotra, B., Srivastava, S., & Augustine, S. (2015). Biosensors for Food Toxin Detection: Carbon Nanotubes and Graphene. *MRS Proceedings, 1725*. doi:10.1557/opl.2015.165

14. C. Gerlach, J. Lange and O. Kanoun, "Carbon nanotube composite for application in gait analysis," *International Multi-Conference on Systems, Sygnals & Devices*, Chemnitz, 2012, pp. 1-4.

15. Chung-Lin Wu, Hsueh-Chu Lin, Jiong-Shiun Hsu, Ming-Chuen Yip, Weileun Fang, Static and dynamic mechanical properties of polydimethylsiloxane/carbon nanotube nanocomposites, Thin Solid Films, Volume 517, Issue 17, 2009, Pages 4895-4901, ISSN 0040-6090, http://dx.doi.org/10.1016/j.tsf.2009.03.146.

16. J. Engel, J. Chen, Nannan Chen, S. Pandya and Chang Liu, "Multi-Walled Carbon Nanotube Filled Conductive Elastomers: Materials and Application to Micro Transducers," *19th IEEE International Conference on Micro Electro Mechanical Systems*, Istanbul, Turkey, 2006, pp. 246-249.

17. Beigbeder, A., Linares, M., Devalckenaere, M., Degée, P., Claes, M., Beljonne, D., Lazzaroni, R. and Dubois, P. (2008), CH-π Interactions as the Driving Force for Silicone-Based Nanocomposites with Exceptional Properties. Adv. Mater., 20: 1003–1007.

18. S. Khan, S. Tinku, L. Lorenzelli and R. S. Dahiya, "Flexible Tactile Sensors Using Screen-Printed P(VDF-TrFE) and MWCNT/PDMS Composites," in *IEEE Sensors Journal*, vol. 15, no. 6, pp. 3146-3155, June 2015.

19. Zhenzhen Quan, Zachary Larimore, Xiaohong Qin, Jianyong Yu, Mark Mirotznik, Joon-Hyung Byun, Youngseok Oh, Tsu-Wei Chou, Microstructural characterization of additively manufactured multi-directional preforms and composites via X-ray micro-computed tomography, Composites Science and Technology, Volume 131, 2016, Pages 48-60, ISSN 0266-3538

20. Hye-Mi So, Jin Woo Sim, Jinhyeong Kwon, Jongju Yun, Seunghyun Baik, Won Seok Chang, Carbon nanotube based pressure sensor for flexible electronics, Materials Research Bulletin, Volume 48, Issue 12, 2013, Pages 5036-5039, ISSN 0025-5408, http://dx.doi.org/10.1016/j.materresbull.2013.07.022.

21. L. Pinna, R. S. Dahiya and M. Valle, "SPICE model for Piezoelectric Bender Generators," *2009 16th IEEE International Conference on Electronics, Circuits and Systems - (ICECS 2009)*, Yasmine Hammamet, 2009, pp. 587-590.

22. C.M. Costa, L.C. Rodrigues, V. Sencadas, M.M. Silva, J.G. Rocha, S. Lanceros-Méndez, Effect of degree of porosity on the properties of poly (vinylidene fluoride–trifluorethylene) for Li-ion battery separators, Journal of Membrane Science, Volume 407, 2012, Pages 193-201, ISSN 0376-7388, http://dx.doi.org/10.1016/j.memsci.2012.03.044.

23. R. S. Dahiya, M. Valle, G. Metta, L. Lorenzelli and S. Pedrotti, "Deposition, processing and characterization of P(VDF-TrFE) thin films for sensing applications," *2008 IEEE Sensors*, Lecce, 2008, pp. 490-493 A strain sensor based on an aligned carbon particle string in a UV-cured polymer matrix

24. Høyer, H., Knaapila, M., Kjelstrup-Hansen, J., Liu, X., & Helgesen, G. (November 21, 2011). A strain sensor based on an aligned carbon particle string in a UV-cured polymer matrix. *Applied Physics Letters, 99,* 21, 213106.

25. Hanwha Chemical, 2017. [Online]. Available: https://hcc.hanwha.co.kr/eng/business/bus_table/nano_02.jsp.

26. S. Khan, L. Lorenzelli and R. S. Dahiya, "Bendable piezoresistive sensors by screen printing MWCNT/PDMS composites on flexible substrates," *2014 10th Conference on Ph.D. Research in Microelectronics and Electronics (PRIME)*, Grenoble, 2014, pp. 1-4.

27. nScrypt Inc, "*3DN HP SERIES*", January 2016. Available: http://www.nscrypt.com/3d-series-equipment/3dn/

28. P. Pa, Z. Larimore, P. Parsons and M. Mirotznik, "Multi-material additive manufacturing of embedded low-profile antennas," in *Electronics Letters*, vol. 51, no. 20, pp. 1561-1562, 10 1 2015.

29. S. Khan, W. Dang, L. Lorenzelli, R. Dahiya Flexible Pressure Sensors Based on Screen-Printed P(VDF-TrFE) and P(VDF-TrFE)/MWCNTs IEEE Trans. Semicond. Manuf., 28 (4) (2015), pp. 486-493

30. G. E. Jabbour, R. Radspinner and N. Peyghambarian, "Screen printing for the fabrication of organic light-emitting devices," in *IEEE Journal of Selected Topics in Quantum Electronics*, vol. 7, no. 5, pp. 769-773, Sep/Oct 2001.

31. Obesity Shipman, A.R. and Millington, G.W.M. (2011), Obesity and the skin. British Journal of Dermatology, 165: 743–750. doi:10.1111/j.1365-2133.2011.10393.x

32. Noah S. Scheinfeld, Obesity and dermatology, Clinics in Dermatology, Volume 22, Issue 4, 2004, Pages 303-309, ISSN 0738-081X, http://dx.doi.org/10.1016/j.clindermatol.2004.01.001.

33. Dowling, A. M., Steele, J. R., & Baur, L. A. (May 31, 2001). Does obesity influence foot structure and plantar pressure patterns in prepubescent children? *International Journal of Obesity, 25,* 6, 845-852.

34. Hills, A. P., Hennig, E. M., McDonald, M., & Bar-Or, O. (October 31, 2001). Plantar pressure differences between obese and non-obese adults: a biomechanical analysis. *International Journal of Obesity, 25,* 11, 1674-1679.

35. William J Jeffcoate, Keith G Harding, Diabetic foot ulcers, The Lancet, Volume 361, Issue 9368, 2003, Pages 1545-1551, ISSN 0140-6736, http://dx.doi.org/10.1016/S0140-6736(03)13169-8.

36. Centers for Disease Control and Prevention. National Diabetes Statistics Report: Estimates of Diabetes and Its Burden in the United States, 2014. Atlanta, GA: US Department of Health and Human Services; 2014.

37. Brem H, Balledux J, Bloom T, Kerstein MD, Hollier L. Healing of Diabetic Foot Ulcers and Pressure Ulcers with Human Skin EquivalentA New Paradigm in Wound Healing. *Arch Surg.* 2000;135(6):627-634. doi:10.1001/archsurg.135.6.627

38. PIC24FJ128GB202 - Microcontrollers and Processors", *Microchip.com*, 2017. [Online]. Available: http://www.microchip.com/wwwproducts/en/PIC24FJ128GB202.

39. Zeller JL, Lynm C, Glass RM. Pressure Ulcers. *JAMA.* 2006;296(8):1020. doi:10.1001/jama.296.8.1020

40. PICkit™ 3 In-Circuit Debugger - PG164130 | Microchip Technology Inc.", *Microchip.com*, 2017. [Online]. Available: http://www.microchip.com/Developmenttools/ProductDetails.aspx?PartNO=PG164130.

41. ALD1116 Datasheet(PDF) - Advanced Linear Devices", *Alldatasheet.com*, 2017. [Online]. Available: http://www.alldatasheet.com/datasheet-pdf/pdf/55018/ALD/ALD1116.html.

42. Bsoul, A.; Mohamed Ali, M.S.; Takahata, K.: 'Piezoresistive pressure sensor using vertically aligned carbon-nanotube forests', Electronics Letters, 2011, 47, (14), p. 807-808, DOI: 10.1049/el.2011.1498

43. Full Spectrum Laser", *Fslaser.com*, 2017. [Online]. Available: https://fslaser.com/Product/Hobby.